Published OnlineFirst May 16, 2018; DOI: 10.1158/0008-5472.CAN-18-0324

Tumor Biology and Immunology

Cancer Research

Long-Chain n-3 Fatty Acids Attenuate Oncogenic KRas-Driven Proliferation by Altering Plasma Membrane Nanoscale Proteolipid Composition

Natividad R. Fuentes[1,2], Mohamed Mlih[3], Rola Barhoumi[4], Yang-Yi Fan[1], Paul Hardin[5], Trevor J. Steele[6], Spencer Behmer[6], Ian A. Prior[7], Jason Karpac[3], and Robert S. Chapkin[1,8]

Abstract

Ras signaling originates from transient nanoscale compartmentalized regions of the plasma membrane composed of specific proteins and lipids. The highly specific lipid composition of these nanodomains, termed nanoclusters, facilitates effector recruitment and therefore influences signal transduction. This suggests that Ras nanocluster proteolipid composition could represent a novel target for future chemoprevention interventions. There is evidence that consumption of fish oil containing long-chain n-3 polyunsaturated fatty acids (n-3 PUFA) such as eicosapentaenoic acid (EPA, $20{:}5^{\Delta 5,8,11,14,17}$) and docosahexaenoic acid (DHA, $22{:}6^{\Delta 4,7,10,13,16,19}$) may reduce colon cancer risk in humans, yet the mechanism underlying this effect is unknown. Here, we demonstrate that dietary n-3 PUFA reduce the lateral segregation of cholesterol-dependent and -independent nanoclusters, suppressing phosphatidic acid-dependent oncogenic KRas effector interactions, via their physical incorporation into plasma membrane phospholipids. This results in attenuation of oncogenic Ras-driven colonic hyperproliferation in both *Drosophila* and murine models. These findings demonstrate the unique properties of dietary n-3 PUFA in the shaping of Ras nanoscale proteolipid complexes and support the emerging role of plasma membrane-targeted therapies.

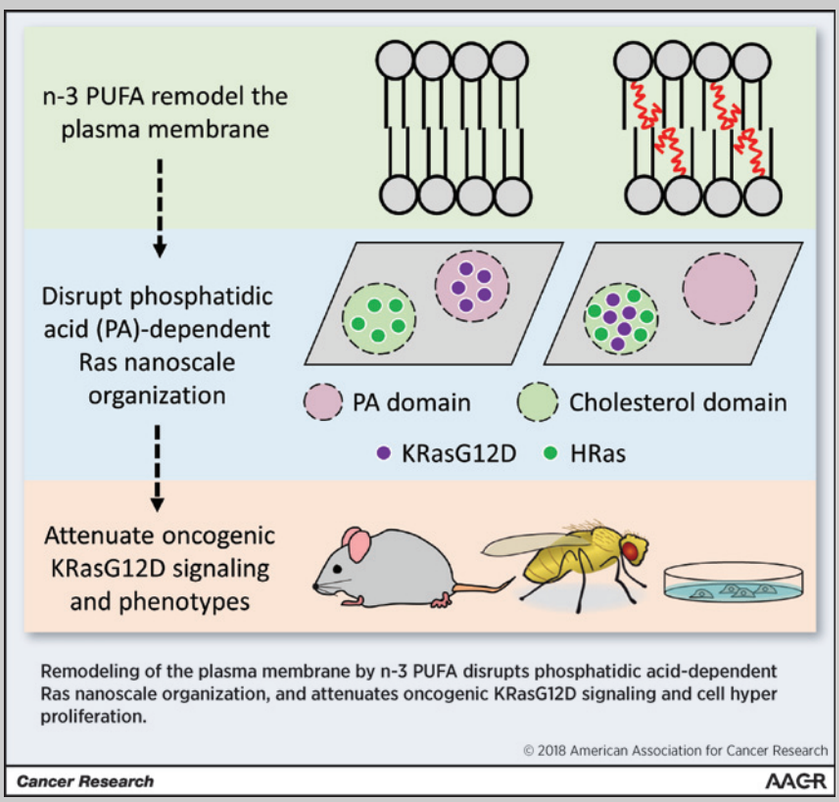

Significance: The influence of dietary long chain n-3 polyunsaturated fatty acids on plasma membrane protein nanoscale organization and KRas signaling supports development of plasma membrane-targeted therapies in colon cancer.

Graphical Abstract: http://cancerres.aacrjournals.org/content/canres/78/14/3899/F1.large.jpg. *Cancer Res; 78(14); 3899–912. ©2018 AACR.*

[1]Program in Integrative Nutrition and Complex Diseases, Texas A&M University, College Station, Texas. [2]Department of Veterinary Physiology and Pharmacology, Texas A&M University, College Station, Texas. [3]Department of Molecular and Cellular Medicine, College of Medicine, Texas A&M Health Sciences Center, College Station, Texas. [4]Department of Veterinary Integrative Biosciences, Texas A&M University, College Station, Texas. [5]Department of Biology, Texas A&M University, College Station, Texas. [6]Department of Entomology, Texas A&M University, College Station, Texas. [7]Division of Cellular and Molecular Physiology, University of Liverpool, Liverpool, United Kingdom. [8]Center for Translational Environmental Health Research, Texas A&M University, College Station, Texas.

Note: Supplementary data for this article are available at Cancer Research Online (http://cancerres.aacrjournals.org/).

Corresponding Authors: Robert S. Chapkin, Program in Integrative Nutrition & Complex Diseases, Texas A&M University, 112 Cater Mattil, TAMU 2253, College Station, TX 77843-2253; E-mail: r-chapkin@tamu.edu

doi: 10.1158/0008-5472.CAN-18-0324

Published OnlineFirst May 16, 2018; DOI: 10.1158/0008-5472.CAN-18-0324

Introduction

Approximately 45% of colorectal cancers harbor KRas mutations (1), which confer resistance to standard therapy (2). Moreover, to date, targeting of mutant Ras proteins in cancers has not been possible (3). A number of Ras effector proteins and cell signaling pathways have been defined, including the Raf and the MAP kinase pathway, the PI3K and the Akt/mTOR pathway, and the RalGDS and Ral pathway. Ras effector proteins physically associate with Ras proteins to propagate signal transduction (4). These signals result in increased proliferation, decreased apoptosis, disrupted cellular metabolism, and increased angiogenesis, all seminal hallmarks of cancer (5). Thus, there is a critical need to develop new KRas-targeted therapeutic approaches with reduced toxicities in the setting of acute or chronic administration.

High-fidelity signaling of KRas is dependent on its spatial organization into defined proteolipid nanoassemblies (6). Recently, it was demonstrated that select amphiphilic agents, through direct modulation of the biophysical properties of the plasma membrane, compromise oncogenic KRas-mediated signal transduction by altering its precise nanoscale membrane organization (7). Furthermore, the paradoxical activation of MAPK signaling by BRaf inhibitors in oncogenic KRas-expressing cells is driven by an increase in KRas nanoassembly clustering (8). These findings suggest that Ras nanoscale proteolipid composition could be a novel therapeutic target (8).

The molecular mechanisms that influence the formation and structure of Ras nanoclusters involve lipid–lipid and protein–lipid interactions between the C-terminal plasma membrane anchor and plasma membrane phospholipids (9). In regard to membrane phospholipids, recent work has shown that nanocluster formation is not only dependent on the charged head groups (10), but also the asymmetry and saturation index of the fatty acyl lipid tail region (11). Interestingly, dietary consumption of long-chain n-3 polyunsaturated fatty acids (n-3 PUFA), such as eicosapentaenoic acid (EPA, $20{:}5^{\Delta5,8,11,14,17}$) and docosahexaenoic acid (DHA, $22{:}6^{\Delta4,7,10,13,16,19}$), results in the incorporation of these fatty acids into cell membrane phospholipids (12). This is noteworthy because the consumption of EPA and DHA may reduce colon cancer risk in humans (13). Hence, establishing a causal role of n-3 PUFA in colon cancer prevention would have a major translational impact because these dietary nutrients are relatively inexpensive, safe and well tolerated (14). However, the molecular mechanisms by which n-3 PUFA specifically impact oncogenic KRas-driven colon cancer remain to be determined. Herein, we report that the incorporation of DHA and EPA into plasma membrane phospholipids (i) modifies KRas nanoscale proteolipid composition, (ii) disrupts oncogenic KRas driven signaling (pERK), and (iii) suppresses KRas associated phenotypes (hyperproliferation) *in vitro* and *in vivo*. Together, these results suggest a unique role for n-3 PUFA in the modulation of KRas nanoscale spatial organization and signaling.

Materials and Methods

Mouse genetics, husbandry, and diet

All animal experiments were approved and conducted in strict accordance with the Texas A&M University Institutional Animal Care and Use Committee, and conformed to NIH guidelines. To generate an inducible colonic targeted oncogenic KRas mouse model (Fig. 1A), CDX2P-CreERT2 mice (RRID:IMSR_JAX:022390) were crossed with LSL-K-ras G12D mice (RRID:IMSR_JAX:008179). Mice were housed in cages in a temperature- and humidity-controlled animal facility with a 12 h light/dark cycle and fed lab chow.

For *in vivo* diet studies, mice were fed experimental diets containing either n-6 (control) or n-3 PUFA for 2 weeks before tamoxifen injection (Fig. 1B). Both diets contained 20% (w/w) casein, 42% sucrose, 22% cornstarch, 6% cellulose, 3.5% AIN-76 mineral mix, 1% AIN-76 vitamin mix, 0.3% methionine, 0.2% choline, and 0.02% tert-Butylhydroquinone (TBHQ). The n-6 diet contained 5% (w/w) corn oil (Dyets, #401150), and the n-3 diet contained 4% menhaden fish oil (Omega Pure) and 1% corn oil. The diets were changed daily and contained TBHQ to prevent peroxidation. Four weeks before termination, mice were injected once intraperitoneally with 200 mg/kg tamoxifen (Sigma-Aldrich, # T5648; ref. 15) dissolved in corn oil (as a carrier) or injected with corn oil alone.

In vivo measurement of crypt proliferation and length

For the purpose of measuring rates of colonic cell proliferation, mice were injected intraperitoneally with 50 mg/kg EdU (Life Technologies, #A10044) 2 hours before termination. At the time of euthanasia, colon tissue was flushed with PBS and the colon was processed to generate Swiss rolls (16). Swiss rolls were subsequently fixed in 4% paraformaldehyde and embedded in paraffin. For cell proliferation assays, formalin-fixed paraffin-embedded 4-μm colon Swiss roll sections were deparaffinized and rehydrated through graded ethanol washes. Cell proliferation in colonic crypts was measured using the Click-iT EdU Alexa Fluor 555 Imaging Kit (Life Technologies, #C10338) as per the manufacturer's instructions (16). Negative control slides were incubated without Alexa Fluor.

For crypt length, tissue sections were stained with Alcian blue and imaged with a Leica Aperio CS2 digital pathology scanner. Crypt measurement was performed using ImageScope (RRID:SCR_014311) software.

Cell culture

Conditionally immortalized young adult mouse colonic (YAMC) cells (RRID:CVCL_6E40) were originally obtained from R.H. Whitehead, Ludwig Cancer Institute (Melbourne, Australia). YAMC cells (passages 14–20) were cultured under permissive conditions, 33°C and 5% CO_2 in RPMI-1640 media (Mediatech) supplemented with 5% FBS (FBS; Hyclone), 2 mmol/L GlutaMax (Gibco), 5 μg/mL insulin, 5 μg/mL transferrin, 5 ng/mL selenious acid (Collaborative Biomedical Products), and 5 IU/mL of murine interferon-γ (Roche). YAMC cells were authenticated (07/24/15) by STR profiling (CellCheck Plus) by IDEXX BioResearch. Isogenic SW48 KRas (G12D/+) cells (RRID:CVCL_LC92) were obtained (10/08/14) from Horizon Discovery, where they were authenticated by gDNA and cDNA genotyping. SW48 cells (passages 8–13) were maintained at 37°C and 5% CO_2 in McCoy's 5A medium supplemented with 10% FBS. DKOB8 cells were acquired (09/19/03) from Dr. Patrick Casey (Duke University, Durham, NC) who maintained them for Dr. Gideon Bollag, Onyx-Pharmaceuticals (San Francisco, California; ref. 17). DKOB8 cells (passages 7–12) were maintained at 37°C and 5% CO_2 in DMEM, high-glucose medium supplemented with 5% FBS. Where indicated, DKOB8 cells were incubated with 10 μmol/L ponasterone A (Thermo Fisher, H10101) for 48 hours, which verifies the cell type by large induction of KRas. All cell

lines used tested negative for *Mycoplasma* bacteria (September 15, 2016) as assessed by a MycoAlert PLUS *Mycoplasma* Detection Kit (Lonza, #LT07-701). Select cultures were treated for 72 hours with 50 μmol/L fatty acid [linoleic acid (LA, 18:2n6), arachidonic acid (AA, 20:4n6), eicosapentaenoic acid (EPA, 20:5n3) or docosahexaenoic acid (DHA, 22:6n3); NuChek, Elysian, MN] complexed with fatty acid–free BSA.

Drosophila genetics, stocks, and culture

The following strains were obtained from the Bloomington *Drosophila* Stock Center: w1118, UAS-Ras^{V12} (BDSC Cat# 64196, RRID:BDSC_64196), and tub-Gal80ts (DGGR Cat# 130454, RRID:DGGR_130454). esg-Gal4 was kindly provided by Dr. Shigeo Hayashi, Riken Center for Developmental Biology. UAS-GFP-tK, UAS-RFP-tK, UAS-GFP-tH, UAS-RFP-tH were kindly provided by Dr. John F. Hancock, University of Texas Health Science Center (Houston, TX; ref. 18). All flies were reared on Bloomington's standard medium at 25°C and 65% humidity on a 12 hours light/dark cycle, unless otherwise indicated. Newly emerged flies were transferred into vials with the test diets and maintained for 5 days.

Drosophila holidic diet

A holidic diet was prepared as previously described (19). Briefly, individual diet components were mixed and prepared in a gel form with agar. Once the diet cooled to <60°C, corn oil (1.79% w/w) or fish oil (1.79% w/w) along with TBHQ (0.02% w/w) was added and the diet was vigorously shaken to ensure uniform mixing, before decanting into plastic feeding tubes. The fatty acid composition of the diets is described in Supplementary Table S1. Newly emerged adult female flies were transferred to diets for 5 days before dissection and the collection of their guts for lipid profiling and imaging. Dietary fish oil was well tolerated, which is consistent with previous studies, demonstrating that dietary long-chain fatty acids are tolerated and readily incorporated into larvae, pupae and adult fly membrane lipids (20, 21).

Conditional expression of UAS-linked transgenes

The esgGal4 driver was combined with a ubiquitously expressed temperature-sensitive Gal80 inhibitor (tubGal80ts). The escargot construct drives expression in stem cells using the EGFR–Ras axis to maintain stemness and suppress differentiation (22). Crosses and flies were kept at 18°C (permissive temperature) and 5-day-old females were fed the test diets 5 days and then shifted to 29°C for 2 days to allow expression of the transgenes before analysis.

Drosophila immunostaining and microscopy

Intact fly guts were fixed at room temperature for 20 minutes in 100 mmol/L glutamic acid, 25 mmol/L KCl, 20 mmol/L $MgSO_4$, 4 mmol/L sodium phosphate, 1 mmol/L $MgCl_2$, and 4% formaldehyde. All subsequent incubations were performed using PBS, 0.5% BSA, 0.1% Triton X-100 at 4°C. The following primary antibodies were used: anti-phospho-Histone H3 (Millipore; 1:1,000), anti-armadillo (1:250 dilution), obtained from the Developmental Studies Hybridoma Bank. Fluorescent secondary antibodies were obtained from Jackson ImmunoResearch. Hoechst dye was used to stain DNA. Confocal images were collected using a Nikon Eclipse Ti confocal system and processed using Nikon software and Adobe Photoshop.

Cell line immunofluorescence

For quantitative phospho-ERK analysis, cells were seeded in cell imaging 8 chamber coverglass slides (Eppendorf, 0030742036) and treated with select fatty acids (50 μmol/L) for 72 hours. Cells were subsequently serum starved (0% FBS) for 18 hours in the presence of fatty acid, stimulated with EGF (25 ng/mL; PeproTech, 315-09) for 5 minutes and immediately fixed in ice-cold 100% methanol. Cells were incubated with primary phospho-ERK (Cell Signaling Technology, #4370, 1:200, RRID:AB_2315112) antibody followed by alexa-647 fluorescent secondary antibody (Jackson ImmunoResearch Labs, #711-605-152, 1:400, RRID:AB_2492288). CellMask Green Plasma Membrane Stain (Thermo Fisher, #C37608, 1:1,000) was used to label the cells and Hoechst 33342 (Thermo Fisher, #H3570, 1:2,000) to label the nucleus. Cells were imaged with a 1.3 numerical aperture ×40 Plan-Fluor oil objective or 1.4 numerical aperture ×100 Plan-Apo oil objective mounted on a wide field Nikon Eclipse microscope using identical settings between samples. For analysis, images were opened in NIH ImageJ software (ImageJ, RRID:SCR_003070; Fiji, RRID:SCR_002285), converted to Tiff files and a custom macro was used to quantify average fluorescent intensity of pERK. Briefly, green membrane stain was used to define a binary cell mask that was applied to pERK images. Average fluorescent intensity of the mask images was subsequently recorded (Supplementary Fig. S1).

For quantitative nuclear pERK to cytoplasmic ratio analysis, images were captured with a 1.15 numerical aperture 40× ACS-Apo oil objective mounted on a Leica DMi8 TCS SPE spectral confocal microscope. After the nuclei were highlighted by Hoechst 33342 (Thermo Fisher, #H3570), NIH ImageJ software (ImageJ, RRID:SCR_003070; Fiji, RRID:SCR_002285) was used to manually define the cytoplasm and nuclear fields of interest. Average intensities were used to quantify the nuclear to cytoplasm ratio.

Western blot analysis of intestinal proteins

For DKOB8 cell Western blotting, cells were homogenized in ice-cold homogenization buffer (50 mmol/L Tris-HCl, pH 7.2, 250 mmol/L sucrose, 2 mmol/L EDTA, 1 mmol/L EGTA, 50 mmol/L sodium fluoride, 1%Triton X-100, Halt Phosphatase Inhibitor Cocktail (Thermo Fisher, #78420), Protease Inhibitor Cocktail (Sigma, #P8340), and 10 mmol/L β-mercaptoethanol. Following homogenization, lysates were sheared using a 29G needle, incubated on ice for 30 minutes, and centrifuged at 16,000 × *g* for 20 minutes. The supernatant was collected and protein concentration was assessed using Coomassie Plus Protein assay (Pierce, #23236). For each sample, 10 μg of protein lysate was treated with 4X Laemmli Sample Buffer (Bio-Rad, #161-0747) and subjected to SDS-PAGE in precast 4% to 20% Mini-PROTEAN TXG Stain-Free Gels (Bio-Rad, #456-8096). After electrophoresis, total protein was activated and visualized with a ChemiDoc Imaging system (Bio-Rad, #17001401) according to the manufacturer's instructions. Subsequently, proteins were electroblotted onto a nitrocellulose membrane with the use of a Trans-Blot Turbo Transfer Pack (Bio-Rad, #1704158) and Trans-Blot Turbo Transfer System (Bio-Rad, #1704150) according to the manufacturer's instructions. Following transfer, total protein was visualized and the membrane was incubated in Membrane Blocking Solution (Thermo Fisher, #000105) at room temperature for 1 hour with shaking, followed by

Published OnlineFirst May 16, 2018; DOI: 10.1158/0008-5472.CAN-18-0324

incubation with shaking overnight at 4°C with primary antibody diluted in Membrane Blocking Solution. Membranes were washed with 0.1% Tween 20 in TBS (TBST) and incubated with secondary peroxidase conjugated secondary antibody as per the manufacturer's instructions. Bands were developed using Clarity Western ECL substrate (Bio-Rad, #170-5060). Blots were visualized using a ChemiDoc Imaging System. Antibodies directed against phospho-ERK (Cell Signaling Technology, #4370; 1:2,000, RRID:AB_2315112), total ERK (Cell Signaling Technology, #4695; 1:1,000, RRID:AB_390779), and Pan-Ras (Millipore Sigma, #OP40; 1:1,000 dilution, RRID:AB_213400) were used. Peroxidase conjugated antibodies goat anti-rabbit IgG (Kirkegaard and Perry Laboratories, #074-1516; 1:20,000) and peroxidase conjugated goat anti-mouse IgG (Kirkegaard and Perry Laboratories, #074-1806; 1:20,000) were used.

For *Drosophila* Western experiments, intact female guts were dissected in cold PBS and proteins extracted in Laemmli buffer, separated on 10% acrylamide gel and transferred according to standard procedures. Antibodies directed against phospho-ERK (Cell Signaling Technology, #4370; 1:1,000), total ERK (Cell Signaling Technology, #4695; 1:1,000), β-actin (Cell Signaling Technology; 1:5,000 dilution, RRID:AB_10950489) were used. Total protein extracts were pooled from 4 guts.

Fluorescence lifetime imaging microscopy combined with fluorescence resonance energy transfer

For *in vitro* FLIM experiments, YAMC cells were seeded at a density of 1×10^4 in cell imaging 8 chamber coverglass (Eppendorf, 0030742036) 24 hours before fatty acid-BSA (50 μmol/L) treatment. Following a 24 hours incubation period, media without fatty acid were added and Lipofectamine 3000 (Thermo Fisher, #L3000-008) was used to transiently transfect cells with plasmids of donor (GFP-tagged protein) alone or cotransfected with FRET acceptors (7, 18). FRET acceptors were RFP-tagged proteins of interest (GFP-: RFP-plasmid at 1:3 ratio, 0.25 μg total plasmid per well). After 8 hours in transfection media, cells were gently washed with PBS and incubated with complete media plus fatty acids for 40 hours. Subsequently, cells expressing GFP-tagged protein alone or coexpressing both GFP-tagged and RFP-tagged proteins were washed with PBS and fixed in 4% PFA for 15 minutes. After three washes in 1× PBS, HPBS was added to wells. The GFP fluorescence lifetime was measured using a Lambert Instrument FLIM unit attached to a wide field Nikon Eclipse microscope. GFP was sinusoidally excited by a modulating 3-Watt 497 nm light-emitting diode (LED) at 40 MHz under epi-illumination. A solution of fluorescein (1 μmol/L) was used as a lifetime reference standard. Cells were imaged with a 1.3 numerical aperture ×40 Plan-Fluor oil objective using an appropriate GFP filter set. The phase and modulation were determined from 12 phase settings using the manufacturer's software. This analysis results in an image where the fluorescence lifetime of GFP is determined and assigned to each pixel. The color scale on each pixel represents the fluorescent lifetime, which equates to the level of interaction between the GFP- and RFP-tagged proteins. Lifetime (phase) values were pooled and averaged from regions of interest drawn on individual cells. Each experiment was replicated at least 2 times. Statistical analysis was performed using one-way ANOVA. The fluorescence lifetime imaging microscopy combined with fluorescence resonance energy transfer (FLIM-FRET) method is highly favored over intensity-based FRET measurements because fluorescent lifetime is an intrinsic property of the fluorescent molecule and is generally insensitive to weak signal, excitation source, and variations in the donor–acceptor ratio (23).

For *Drosophila* FLIM experiments, adult flies expressing GFP/RFP constructs in gut stem cells were dissected in PBS and fixed 20 minutes in 4% PFA before mounting in Mowiol medium. Fields of view were scanned with an inverted LSM 780 microscope (Carl Zeiss Microimaging) and a 1.4 numerical aperture 40 × Plan Apochromat oil objective. Two-photon excitation was provided by a Chameleon (Coherent Inc.) Ti:sapphire laser tuned to 900 nm. Emission events were registered with FastFLIM system (ISS). Fluorescence lifetime images (256 × 256 pixels) were acquired with a pixel dwell time of 6.3 μs. Lifetime of the imaged samples was determined with the frequency domain technique using the ISS VistaVision Suite version 4.1. At least 10 images were collected per treatment.

The percentage of the apparent FRET efficiency (E_{app}) was calculated using the measured lifetimes of each donor–acceptor pair (τ_{DA}) and the average lifetime of the donor-only (τ_D) samples. The formula employed was $E_{app} = (1\text{-}\tau_{DA}/\tau_D) \times 100\%$ (24).

Lipid extraction and fatty acid analysis

For assessment of dietary lipid incorporation into membrane phospholipids, total lipids were extracted from isolated mouse crypts (25) and at least 28 dissected *Drosophila* guts per treatment with 2:1 (v/v) chloroform-methanol as described previously (26). Total phospholipids were subsequently separated by thin-layer chromatography with 90:8:1:0.8 (v/v/v/v) chloroform–methanol–acetic acid–water. After transesterification using methanolic HCl, fatty acid methyl esters were quantified by capillary gas chromatography-mass spectrometry (26).

Lipid add-back

18:0–18:1 phosphatidic acid (#840861, 10 mg/mL in chloroform) and 18:0–18:1 phosphatidylserine (#840039, 10 mg/mL in chloroform) were obtained from Avanti Polar Lipids, dried under nitrogen gas, resuspended in 10 mmol/L in 150 mmol/L NaCl and 10 mmol/L Tris·HCl, pH 8, immediately added to cultures at 100 μmol/L final concentration and incubated for 45 minutes before cell fixation.

Results

Dietary n-3 PUFA ameliorate oncogenic $KRas^{G12D}$-mediated colonic phenotypes *in vivo*

We previously demonstrated that n-3 PUFA suppress intestinal wild type Ras activation both *in vitro* and *in vivo*, by upstream disruption of EGFR function (25, 27). However, oncogenic Ras contains a mutation that essentially keeps it in the active GTP-bound state (1), which renders it insensitive to upstream EGFR inhibition by anti-EGFR therapies (3). To determine whether dietary n-3 PUFA can suppress oncogenic Ras-mediated colonic phenotypes, we used an inducible genetic model of oncogenic KRas-driven colonic hyperproliferation targeted to the colon (Fig. 1A; ref. 15). Following tamoxifen injection, Cre-mediated recombination targeted to the epithelium of the distal ileum, cecum, colon, and rectum removes transcriptional stop elements, resulting in expression of the mutant *Kras* allele under the control of its endogenous

Published OnlineFirst May 16, 2018; DOI: 10.1158/0008-5472.CAN-18-0324

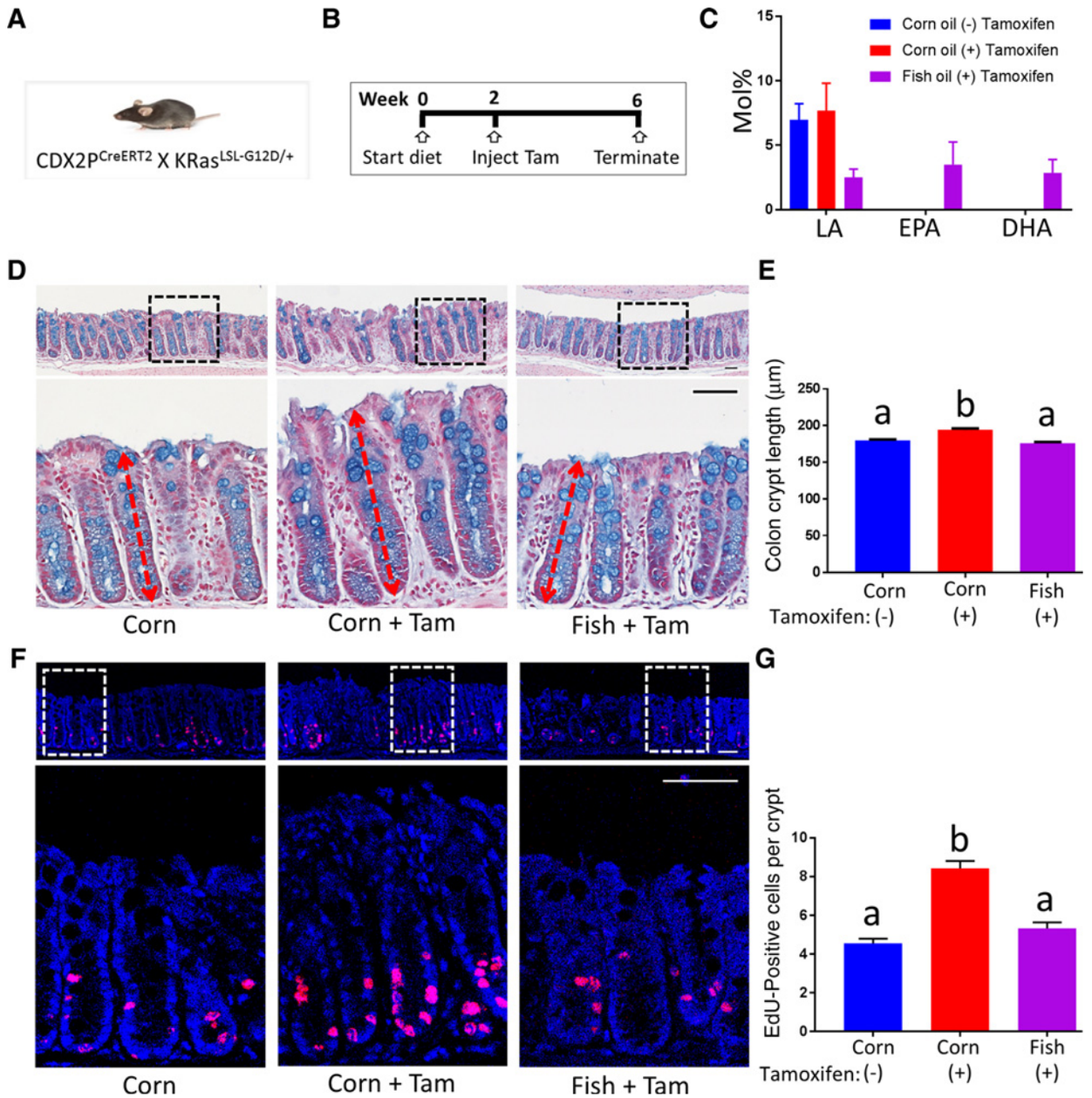

Figure 1.

Dietary n-3 PUFA ameliorates oncogenic KRas^{G12D}-mediated colonic phenotypes. **A** and **B,** Genetic mouse model (**A**) and experimental design (**B**) to determine the efficacy of dietary intervention on oncogenic KRas^{G12D}-driven hyperproliferation in the colon. **C,** Isolated colonic crypt phospholipid profile from mice fed the experimental diets. **D,** Alcian blue-staining of colonic crypts, including high magnification of crypts in dashed black box, with red dashed arrow representing crypt length. **E,** Quantitative analysis of crypt length. Scale bar, 50 μm. **F,** Nuclei (blue) and EdU-labeled (red) proliferating colonocytes in mice 4 weeks post tamoxifen (Tam, 200 mg/kg) fed corn- or fish oil-containing diets. High magnification of crypts is shown in each dashed white box. **G,** Quantitative analysis of cell proliferation. Scale bar, 50 μm. Statistical significance between treatments as indicated by different letters ($P < 0.05$) was examined using one-way ANOVA and uncorrected Fisher LSD tests (**E,** $n = 4$ mice per group and at least 508 crypts counted; **G,** $n = 4$ mice per group and 200 crypts counted).

regulatory elements (15). Mice were fed a diet containing corn (n-6 PUFA control) or fish oil, containing EPA and DHA (Supplementary Tables S2 and S3) for 2 weeks before tamoxifen induction of oncogenic KRas, and maintained for an additional 4 weeks (Fig. 1B). Corn oil contains linoleic acid (LA, 18:2$^{\Delta 9,12}$) that serves as a control for the nonspecific effects of PUFA. The fish oil dose is comparable with a diet containing approximately 8.6 g/d n-3 PUFA in humans (28). We have previously demonstrated that this dose is well-tolerated and mice exhibit no signs of toxicity (25). As expected,

Published OnlineFirst May 16, 2018; DOI: 10.1158/0008-5472.CAN-18-0324

mice fed a diet containing n-3 PUFA exhibited an enrichment of EPA and DHA in membrane phospholipids (Fig. 1C; Supplementary Table S4). Dietary n-3 PUFA treatment substantially reduced the colonic hyperproliferation induced by oncogenic KRas, as indicated by the significant ($P < 0.05$) reduction of crypt length (Fig. 1D and E) and number of EdU positive proliferative cells per crypt (Fig. 1F and G). Collectively, these findings demonstrate that dietary fish oil containing EPA and DHA can attenuate oncogenic KRas-driven colonic phenotypes *in vivo*.

Long-chain n-3 PUFA reshape plasma membrane nanoscale organization of cholesterol dependent and independent nanoclusters

Previous experiments conducted by our laboratory using immuno-gold electron microscopy of plasma membrane sheets suggest that plasma membrane organization of inner leaflets is fundamentally altered by EPA and DHA (29, 30). Specifically, n-3 PUFA treatment altered the nanoscale organization of cholesterol-dependent (tH) and cholesterol-independent (tK) probes expressed in cervical adenocarcinoma (HeLa) and colorectal carcinoma (HCT-116) cells (29, 30). These probes are composed of a fluorescent tag attached to the minimal membrane anchor of HRas (tH-GFP) or KRas (tK-RFP), which targets them to their respective membrane domains (31). In the present study, we monitored the nanoscale organization of cholesterol sensitive (tH) and insensitive (tK) probes by fluorescence lifetime imaging combined with fluorescence resonance energy transfer (FLIM-FRET) microscopy (9). When coexpressed with a corresponding FRET pair, such as RFP, a reduction of GFP lifetime is indicative of more extensive FRET as a result of a smaller distance between GFP and RFP, which is correlated with more extensive nanoclustering (Fig. 2A). Lifetime values were then converted to apparent FRET efficiency percentage, where an increase is indicative of enhanced nanoclustering (24). Importantly, transient expression of these probes faithfully reports on their fraction in nanoclusters, as this remains constant over a multi-log range of expression levels (6). To explore the effects of n-3 PUFA on cholesterol-dependent and -independent nanoclustering, we used immortalized YAMC cells, which express wild-type Ras. This model faithfully recapitulates n-3 PUFA *in vivo* effects (25, 27, 32) and allows for lipidomic and proteomic studies under well-controlled conditions (33). Cells were treated with a physiologically relevant level (50 μmol/L; ref. 34) of albumin-complexed n-3 PUFA (EPA, DHA) or control long-chain n-6 PUFA linoleic acid (LA) for 72 hours. BSA-complexed fatty acids were used to represent the non-esterified fatty acids that are bound to albumin *in vivo*. We have previously demonstrated that this dose is well-tolerated and cells exhibit no signs of toxicity (32). In addition, mevastatin, an HMG-CoA inhibitor was used as a positive control to reduce nanoclustering of Ras and FRET efficiency by blocking farnesylation, and thus membrane anchorage of Ras (24). Interestingly, n-3 PUFA significantly increased ($P < 0.05$) the clustering of tK-GFP (Fig. 2B and C) whereas tH-GFP (Fig. 2D and E) clustering was reduced ($P < 0.05$) compared with untreated control. Because a reduction in FRET can result from disruption of Ras membrane nanoclustering as well as loss of membrane attachment (24), it is noteworthy that the plasma membrane association of tH-GFP but not tK-GFP is reduced following n-3 PUFA treatment (33).

n-3 PUFA are known to modulate differences in membrane rigidity between cholesterol-rich functional microdomains (lipid raft) and non-raft domains (35); thus, we sought to determine whether EPA and/or DHA could alter the lateral segregation of normally spatially separated cholesterol-dependent (tH-GFP) and -independent (tK-GFP) nanoclusters. This outcome would result in the formation of mixed heterotypic nanoclusters, as observed with certain nonsteroidal anti-inflammatory drugs (7). Interestingly, EPA and DHA significantly increased ($P < 0.05$) the formation of heterotypic clustering, as did LA to a lesser extent (Fig. 2F and G). Because the precise nanoscale organization of the minimal membrane anchor of KRas does not completely reflect the localization of its full-length oncogenic constitutively activated counterpart (31, 36), we performed similar heteroclustering experiments with the clinically relevant full-length form of oncogenic KRas. Our results show that EPA and DHA significantly increased the formation of full-length oncogenic KRas and truncated HRas heteroclusters. In contrast, the n-6 PUFA control (LA) had no significant effect (Fig. 2H and I). Taken together, these data demonstrate that the incorporation of n-3 PUFA into plasma membrane phospholipids reshapes the nanoscale organization of cholesterol-dependent and -independent nanoclusters, contributing to the generation of mixed nanoclusters of proteins that are normally segregated and spatially distinct.

Long-chain n-3 PUFA attenuate oncogenic KRas-mediated ERK signaling

We next determined the functional consequences of n-3 PUFA–induced nanoscale reorganization of the plasma membrane by examining oncogenic Ras-dependent signaling. For this purpose, we used a human colon cancer SW48 cell line–expressing mutated KRas. To limit the confounding effects associated with overexpression of oncogenic Ras (37), these cells were designed to express one copy of the mutated KRas variant G12D from the endogenous KRas locus. This particular KRas variant was chosen because one third of colorectal tumors harbor *KRAS* mutations and approximately 80% of these mutations are at codon 12, while the remaining mutations are at codon 13 (38). Because physiological expression of oncogenic KRas does not result in large increases in phosphorylation of ERK, we opted to stimulate cells with EGF (37). Incubation with EPA and DHA in comparison with untreated control reduced ($P < 0.05$) EGF induced ERK phosphorylation by approximately 21% and 33%, respectively (Fig. 3A and B). In contrast, the n-6 PUFA control (LA) had no effect compared with untreated control (Fig. 3B).

To ensure that the observed effect of n-3 PUFA reducing pERK levels was directly caused by disruption of Ras signaling and not an upstream modulator such as EGFR (27), we used an oncogenic KRas inducible cell line, DKOB8. These cells were generated by replacing the original mutated KRas allele in DLD-1 cells with a mutated $KRas^{G12D}$ allele under the control of the ecdysone-inducible vector system (17). This system allows for conditional expression of oncogenic KRas in the presence of ponasterone A, an analog of the insect steroid ecdysone (Supplementary Fig. S2). Cells incubated with ponasterone A with and without fatty acid treatment exhibited an increase in pERK in the DKOB8 $KRas^{G12D}$ overexpression model as determined by immunofluorescence (Fig. 3C and D) and Western blot (Supplementary Fig. S2). Because

Published OnlineFirst May 16, 2018; DOI: 10.1158/0008-5472.CAN-18-0324

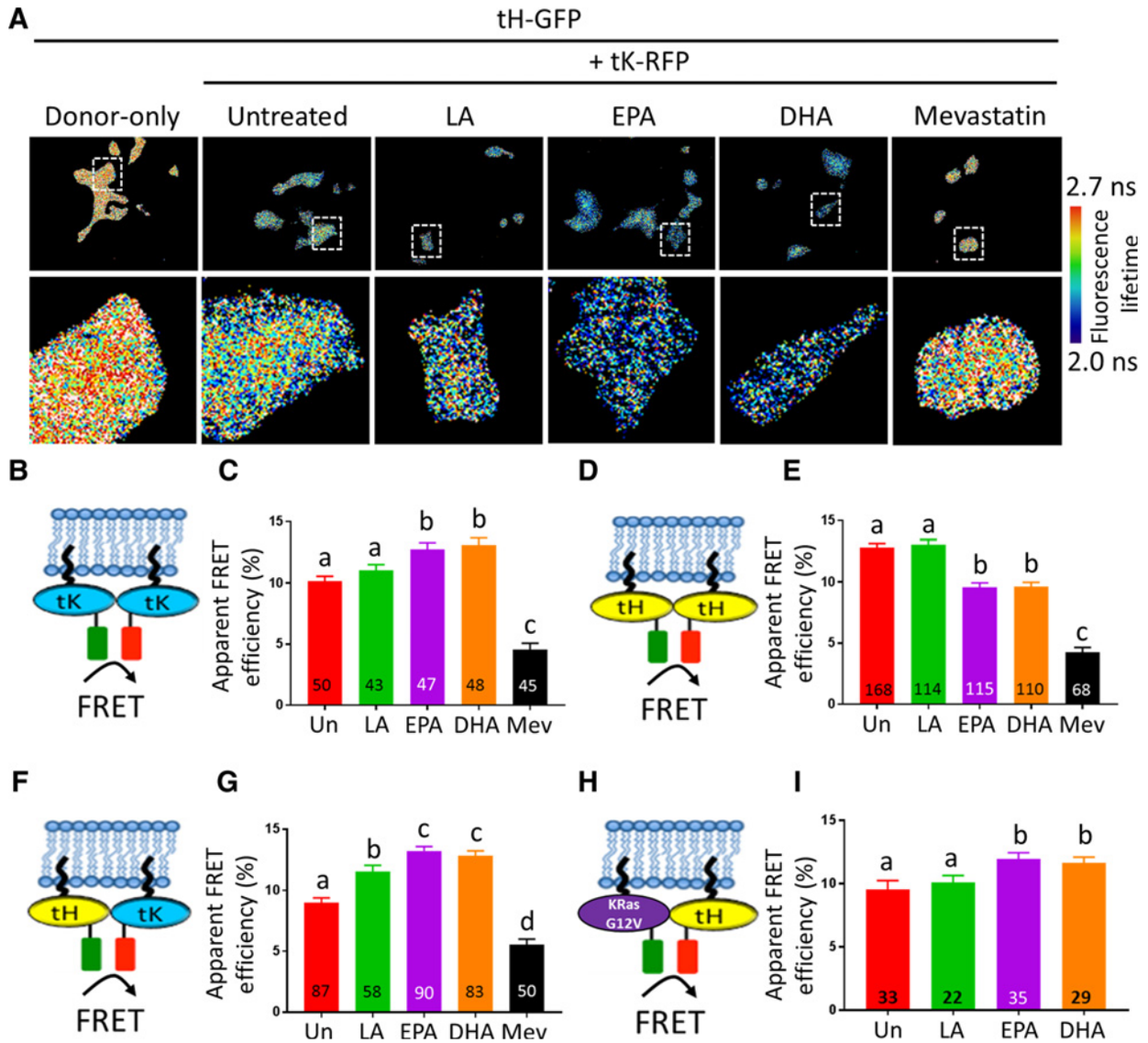

Figure 2.

Long-chain n-3 PUFA disrupts Ras spatiotemporal dynamics. Nanoclustering-FRET analysis (illustrated in schemes) in YAMC cells coexpressing GFP- (**A**) and RFP-tagged truncated KRas (tK; **B**), truncated HRas (tH; **D**), tH-GFP and tK-RFP (**F**), or full-length oncogenic $KRas^{G12V}$-GFP and tH-RFP (**H**). **A,** Representative examples of FLIM-FRET images of YAMC cells from the different FRET samples as indicated. High magnification of cells is shown in each dashed white box. **C**, **E**, **G,** and **I,** YAMC cells were treated with mevastatin (Mev, 5 μmol/L) or indicated fatty acids (50 μmol/L) for 24 or 72 hours, respectively. Cells were transfected 48 hours before imaging. In all graphs (**C**, **E**, **G**, and **I**), the apparent FRET efficiency was calculated from FLIM data (mean ± SEM; $n = 2$–3 independent experiments). Values in the bars indicate the number of cells examined. Statistical significance between treatments as indicated by different letters ($P < 0.05$) was examined using one-way ANOVA and uncorrected Fisher LSD tests. Un, untreated cells.

translocation of pERK from the cytoplasm to the nucleus is required for mitogen-induced cell proliferation (39, 40), in complementary experiments, ERK activation and location were assessed by determining the ratio of active pERK in the nucleus versus the cytoplasm using quantitative immunofluorescence (Fig. 3E). DHA and EPA reduced ($P < 0.05$) oncogenic KRas-driven nuclear pERK accumulation in the DKOB8 model as compared with untreated and n-6 PUFA–treated (LA) cells (Fig. 3E and F).

Dietary n-3 PUFA reshape the nanoscale organization of sterol-dependent and -independent nanoclusters and suppress oncogenic Ras-mediated hyperproliferation in *Drosophila* intestinal stem cells

It is widely reported that a disconnect can occur between cell culture and *in vivo* systems. This is an especially challenging problem in the fields of cancer biology and nutrition, where complex cellular interactions govern the phenotypic outcome. To resolve this inconsistency, we further examined the membrane

Published OnlineFirst May 16, 2018; DOI: 10.1158/0008-5472.CAN-18-0324

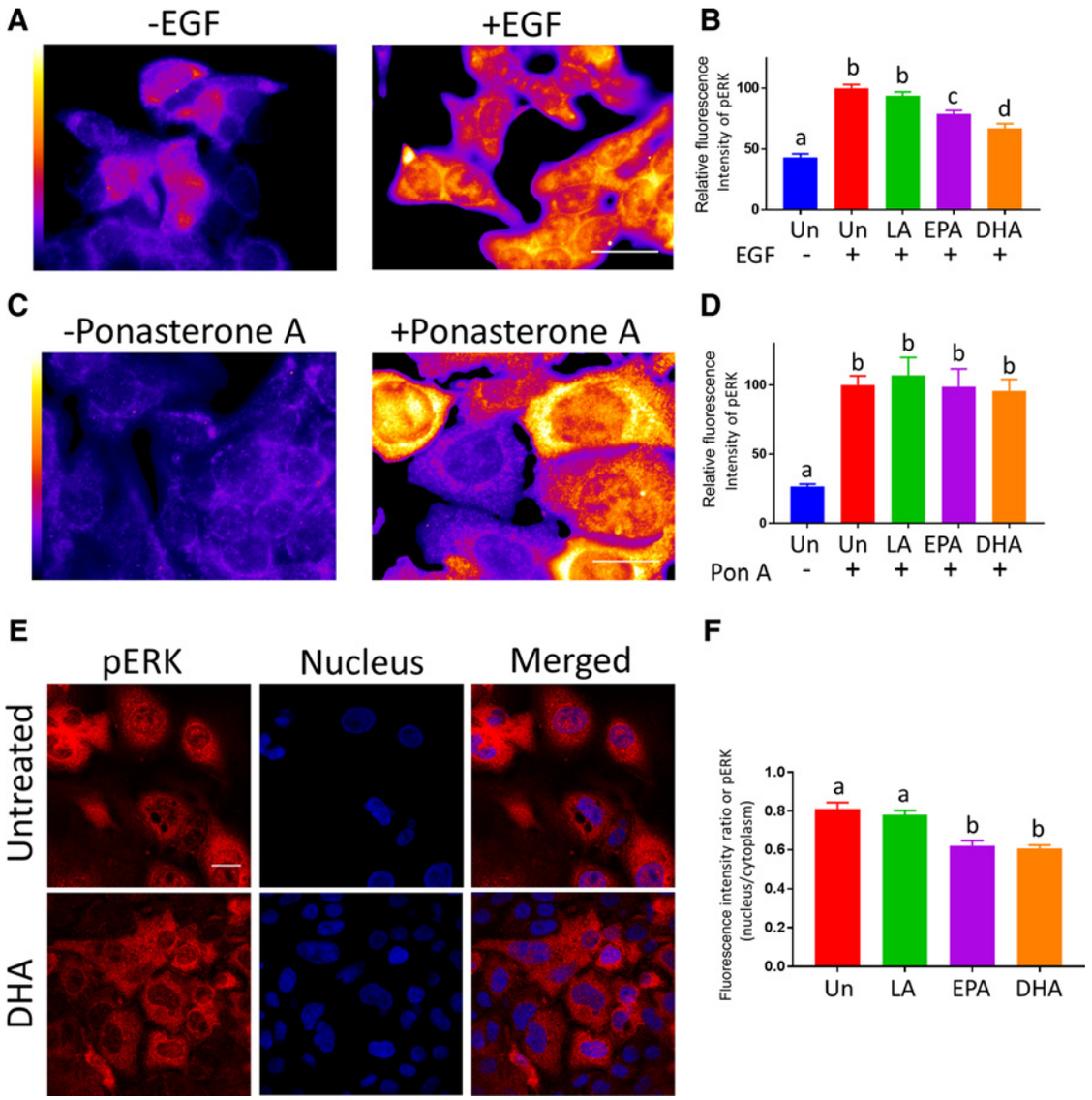

Figure 3.

Long-chain n-3 PUFA attenuates Ras-mediated ERK signaling. **A** and **C,** SW48-KRas^{G12D} (**A**) or DKOB8 (**C**) cells were grown in 8-well glass bottom dishes and treated with 50 μmol/L indicated fatty acid for 72 hours. **A,** SW48-KRas^{G12D} cells were serum starved (0% FBS) over the final 18 hours in the presence of fatty acid and stimulated with EGF (25 ng/mL) for 5 minutes, then immediately fixed in ice-cold 100% methanol. **C,** DKOB8 cells were incubated with ponasterone A (10 μmol/L) for the final 48 hours, and were serum starved (0% FBS) over the final 18 hours in the presence of fatty acid and ponasterone A, then immediately fixed in ice cold 100% methanol. Masked images of pERK ± EGF (**A**) or ± ponasterone A (**C**); scale bar, 20 μm. **B** and **D,** Average fluorescence intensity for pERK. Data represent average fluorescence intensity from at least 10 fields of view, with approximately 10 to 30 cells per field, from three independent experiments. **E,** Representative immunofluorescence confocal images of DKOB8 cells stained for pERK (red) and nuclei (blue). **F,** Quantification of the ratio of fluorescence intensity of pERK in the nucleus versus cytoplasm. Data represent average fluorescence intensity ratio of nucleus to cytoplasm for at least 90 cells, from three independent experiments. Statistical significance between treatments as indicated by different letters ($P < 0.05$) was examined using one-way ANOVA and uncorrected Fisher LSD tests. Un, untreated cells.

altering properties of n-3 PUFA on functional phenotypic and mechanistic Ras clustering outcomes *in vivo*. For this purpose, we used the *Drosophila* intestinal (midgut) epithelium model. The presence of somatic intestinal stem cells (ISC) within the fly midgut allows for the use of a wide range of genetic tools to assay signaling events that govern proliferative homeostasis *in vivo* (41). This barrier epithelia, with functional and morphological similarities to the mammalian small intestine and mouse airway epithelia (41), contains ISCs that can asymmetrically divide, forming an enteroblast (EB) that directly differentiates into functional enterocytes (Fig. 4A). Thus, the *Drosophila* ISC lineage provides an excellent model to study signaling mechanisms regulating stem cell maintenance and dysfunction, including Ras-mediated proliferative signaling (41, 42).

Published OnlineFirst May 16, 2018; DOI: 10.1158/0008-5472.CAN-18-0324

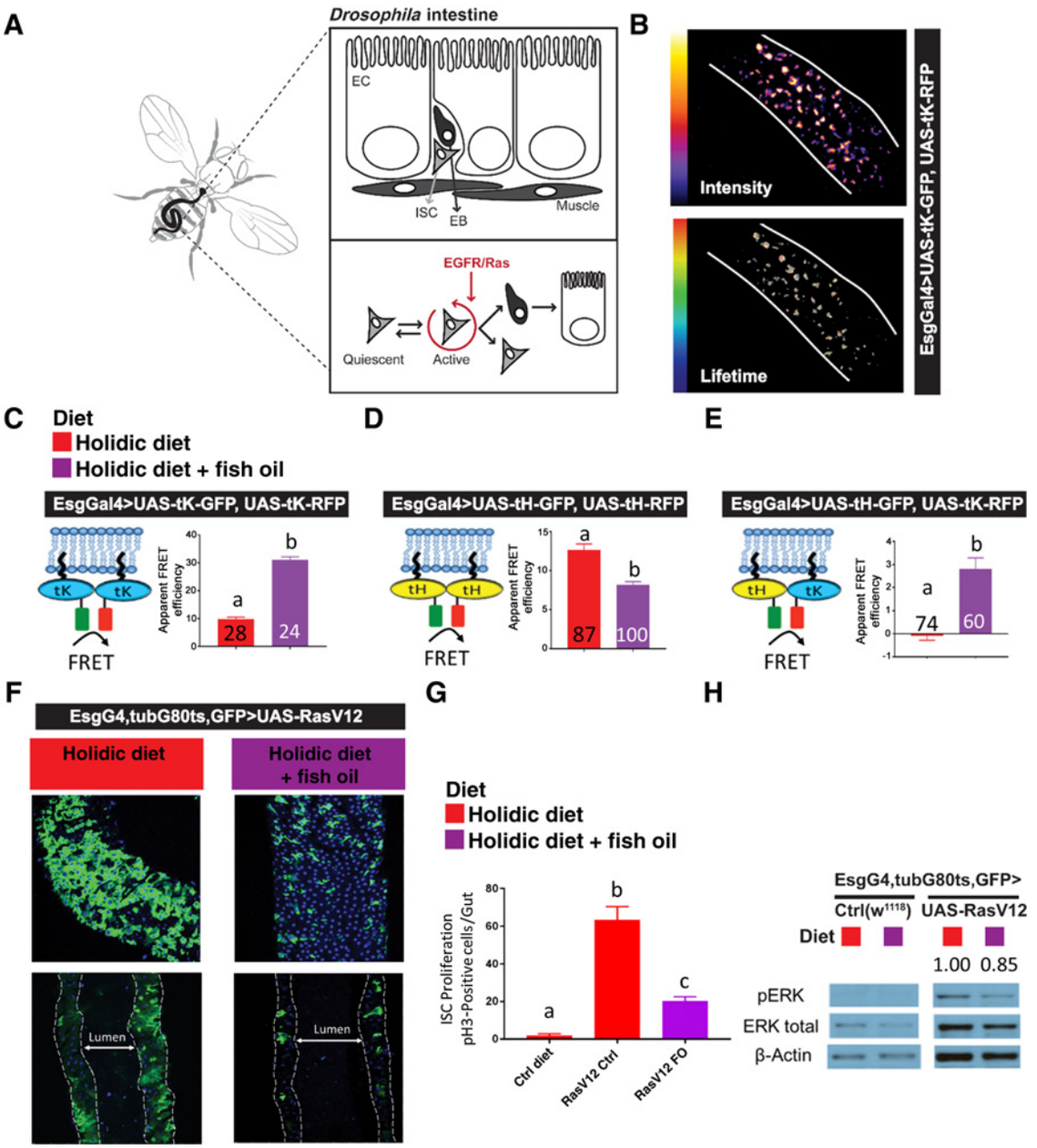

Figure 4.

Dietary n-3 PUFA disrupts Ras spatiotemporal dynamics, suppressing oncogenic Ras-driven hyperproliferation phenotype and signaling in *Drosophila* midguts. **A,** Schematic diagram of *Drosophila* intestine. **B,** Representative intensity and lifetime field of view images of *Drosophila* midguts. Nanoclustering-FRET analysis (illustrated in schemes) in *Drosophila* midgut stem cells coexpressing GFP- and RFP-tagged truncated K-Ras (tK; **C**), truncated H-Ras (tH; **D**) or tH-GFP and tK-RFP (**E**). **C–E,** One- to 2-days-old *Drosophila* were placed on holidic diet containing no lipid (red) or fish oil (purple) for 5 days before dissection and mounting of midguts for microscopy. In all graphs (**C**, **D,** and **E**), the apparent FRET efficiency was calculated from FLIM data (mean ± SEM; $n = 2$ independent experiments). Values in the bars indicate the number of analyzed field of views. Induction of oncogenic RasV12 in *Drosophila* midgut stem cells resulted in hyperproliferation (**F**) at 24 hours and luminal thickening at 48 hours. *Drosophila* fed a fish oil versus control holidic diet for 5 days before induction of oncogenic RasV12 in midgut stem cells exhibited reduced hyperproliferation and midgut luminal thickening. **G,** Quantitative analysis of proliferation as assessed by pH3 at 48 hours post RasV12 induction. **H,** After 24 hours RasV12 induction, guts were harvested and used to assess pERK by Western blot. Statistical significance between treatments as indicated by different letters ($P < 0.05$) was examined using an unpaired *t* test.

Initially, to extend our findings in YAMC cells, we assessed the effects of a fish oil–enriched diet containing n-3 PUFA on sterol-dependent and -independent nanoclusters in *Drosophila* using transgenic flies that express Ras FRET pair constructs (UAS-GFP/RFP-truncated KRas and/or UAS-GFP/RFP-truncated HRas; ref. 18) specifically within ISCs/EBs (using the

Table 1. Incorporation of exogenous fatty acids into *Drosophila* gut membrane phospholipids

Fatty acid	Holidic control (mol%)	Fish oil (mol%)
14:0	4.62	3.07
16:0	11.62	22.79
16:1n-7	35.68	20.71
18:0	3.36	3.47
18:1n-9	36.77	32.19
18:1n-7	0.00	1.94
18:2n-6 (LA)	3.60	4.73
20:0	3.28	1.77
20:4n-6	0.46	0.00
20:5n-3 (EPA)	0.00	5.47
22:0	0.62	0.80
22:6n-3 (DHA)	0.00	1.12

NOTE: Values represent means from pooled *Drosophila* guts ($n = 51$ for control; $n = 46$ for fish oil) grown in two separate vials. Only selected fatty acids in which at least one observation was >0.2 mol% are reported.

EsgGal4 driver). Similar to previous *in vitro* cell culture experiments, control flies expressing only the UAS-GFP–truncated KRas/esgGal4 stem cell driver (lacking the FRET pair; establishes baseline lifetime of GFP with no FRET interaction) or UAS-GFP/RFP–truncated HRas/esgGal4 (used to comparatively determine treatment effects on clustering of truncated HRas) were also assessed. Flies were fed a chemically defined holidic diet (19) that allowed for precise control over all ingredients. The experimental diet differed from the control diet only in its lipid profile—fish oil at 1.79% (w/w; Supplementary Table S1). Phospholipid analysis of the midgut indicated that EPA, and to a lesser extent DHA, was enriched in flies feeding on the n-3 PUFA-enriched diet (Table 1). Using these dietary and genetic conditions, we then performed FLIM-FRET to monitor truncated H- and KRas nanoclustering in *Drosophila* ISCs/enteroblasts. Consistent with our *in vitro* nanoclustering data (Fig. 2B–G), flies on the fish oil diet had increased tK clustering, reduced tH clustering and increased formation of heterotypic clustering (Fig. 4B–E). In a complementary set of experiments, flies were fed an additional n-6 PUFA control diet containing equal amounts of lipid (corn oil; Supplementary Table S1). This resulted in a dramatic increase in LA-containing phospholipids (Supplementary Table S5); however, no effect on tK or tH clustering was observed (Supplementary Fig. S3). Finally, we examined the effect of dietary n-3 PUFA on oncogenic Ras-mediated phenotypes originating from stem cells in the *Drosophila* midgut. For this purpose, the expression of oncogenic RasV12 was targeted to ISCs in the adult fly, which leads to stem cell hyperproliferation and intestinal dysplasia (Fig. 4F; ref. 42). Flies fed n-3 PUFA vs. control exhibited a reduction in stem cell hyperproliferation, luminal thickening/tissue dysplasia (Fig. 4F and G) and ERK activation (Fig. 4H). Collectively, these data demonstrate that dietary fish oil results in the incorporation of n-3 PUFA into plasma membrane phospholipids in *Drosophila* midguts, which is associated with the reshaping of sterol-dependent and -independent nanoclusters, and the amelioration of oncogenic Ras-dependent signaling and hyperproliferation *in vivo*.

Long-chain n-3 PUFA modify oncogenic KRas proteolipid nanoassembly composition

We next sought to determine the mechanism by which n-3 PUFA disrupt cholesterol-dependent and -independent lateral segregation, resulting in a reduction in ERK signaling. Because recruitment of the effector Raf to active Ras proteolipid assemblies is a requirement of the RAS/ERK signal cascade, this effector recruitment can be monitored by coexpression of full-length activated KRasG12V with the Ras-binding domain (RBD) of the effector C-Raf (6). Similar to previous experiments, YAMC cells were treated with PUFA (50 μmol/L) for 72 hours. EPA and DHA reduced the FRET signal between full-length active $KRas^{G12V}$ and the RBD, whereas LA had no effect compared with untreated control (Fig. 5A and B). The dose-dependent effect of DHA on the suppression of Raf effector recruitment is shown in Fig. 5C and D.

Raf effectors contain lipid-binding domains that drive interactions with specific lipids, such as phosphatidylserine (PS) and phosphatidic acid (PA; refs. 43, 44). Active KRas proteolipid complexes concentrate specific lipids (PA and PS) and segregate others (cholesterol) to facilitate efficient effector recruitment, and therefore signal transduction (9, 36, 45, 46). Thus, we assessed the effects of n-3 PUFA on the lipid composition of oncogenic KRas proteolipid assemblies using FLIM-FRET in YAMC cells transiently coexpressing full-length activated $KRas^{G12V}$ and fluorescently tagged lipid-binding domains for PS (LactC2-RFP) or PA (Spo20-RFP). None of the fatty acid treatments tested had an effect on the interaction of PS with $KRas^{G12V}$ (Fig. 5E and F). In contrast, EPA and DHA reduced the interaction of PA with KRasG12V (Fig. 5G and H). Importantly, addition of exogenous PA but not PS to DHA-treated cells restored oncogenic KRasG12V-mediated RBD recruitment (Fig. 5I).

KRasG12V is typically not localized to cholesterol-rich domains, as these domains are suboptimal for Raf activation (36, 46). Thus, it is noteworthy that DHA increased the association of KRasG12V with the cholesterol marker D4H (Fig. 5J and K). These data suggest that DHA treatment mislocalizes activated KRasG12V into a cholesterol-rich domain, which likely contains inactivated H-Ras (Fig. 2I). Furthermore, in DHA-treated cells, exogenous PA restored the lateral segregation of KRasG12V away from the cholesterol marker D4H, whereas PS only partially rescued the structural organization of the membrane (Fig. 5K). Interestingly, incubation of DHA-treated cells with either PA or PS failed to restore the lateral segregation of KRasG12V and the cholesterol-dependent tH domain (Fig. 5L). These observations indicate that membrane enrichment of DHA results in the redistribution of PA in the plasma membrane inner leaflet, which in turn disrupts the nanoscale organization and function of oncogenic KRas proteolipid signaling complexes.

Discussion

Here, we provide evidence that a diet containing long-chain n-3 PUFA, for example, EPA and DHA, attenuates oncogenic Ras signaling and phenotype (hyperproliferation) by altering its nanoscale proteolipid interactions at the plasma membrane (Fig. 6A). To our knowledge, this is the first *in vivo* evidence that dietary bioactives can fundamentally alter Ras membrane nanoscale organization and signaling in the intestine. This is highly relevant since no curative treatments for KRas-driven cancer are available. From a translational and feasibility perspective, these findings lay the foundation for the development of toxicologically innocuous KRas therapeutic approaches. Our data suggest that membrane therapy as a strategy likely requires

Published OnlineFirst May 16, 2018; DOI: 10.1158/0008-5472.CAN-18-0324

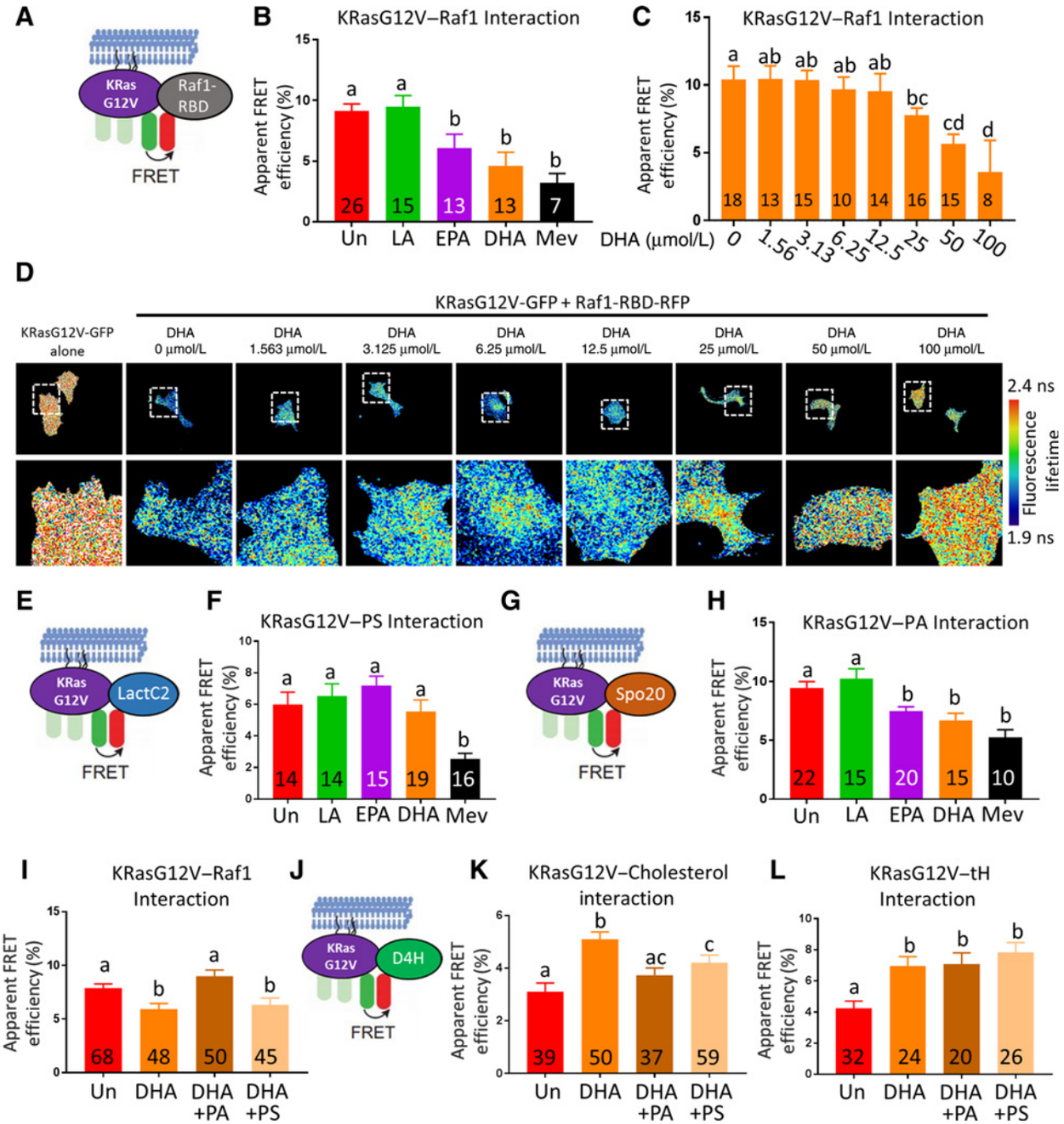

Figure 5.

Long-chain n-3 PUFA alters oncogenic KRasG12V proteolipid composition. Nanoclustering-FRET analysis (illustrated in scheme) in YAMC cells coexpressing full-length oncogenic KRasG12V-GFP and Raf-(R59A)-RBD-RFP (**A**), LactC2-RFP (**E**), Spo20-RFP (**G**), or D4H-RFP (**J**). **B**, **C**, **F**, **H**, **I**, **K,** and **L,** YAMC cells were transfected with KRasG12V-GFP (Donor) alone or cotransfected with indicated RFP tagged probe (Acceptor), and after 48 hours fixed in 4% PFA. Where indicated, cells were untreated or treated with indicated fatty acid (50 μmol/L) for 72 hours and 100 μmol/L PA (18:0-18:1, Avanti #840861) or PS (18:0-18:1, Avanti #840039) for 45 minutes before fixation. Values in the bars indicate the number of cells examined. Statistical significance between treatments as indicated by different letters ($P < 0.05$) was examined using one-way ANOVA and uncorrected Fisher LSD tests. **D,** Representative examples of FLIM-FRET images of YAMC cells from the different FRET samples as indicated. High magnification of cells is shown in each dashed white box. Un, untreated cells; Mev, mevastatin.

the long-term shaping of cellular phospholipids and hence their resident proteins (28). The use of a prolonged regimen as a therapeutic strategy would ideally need to exhibit little or no adverse effects. From a human dose perspective, EPA and DHA administration as high as 17.6 g/day has been shown to be safe and well tolerated (47).

Published OnlineFirst May 16, 2018; DOI: 10.1158/0008-5472.CAN-18-0324

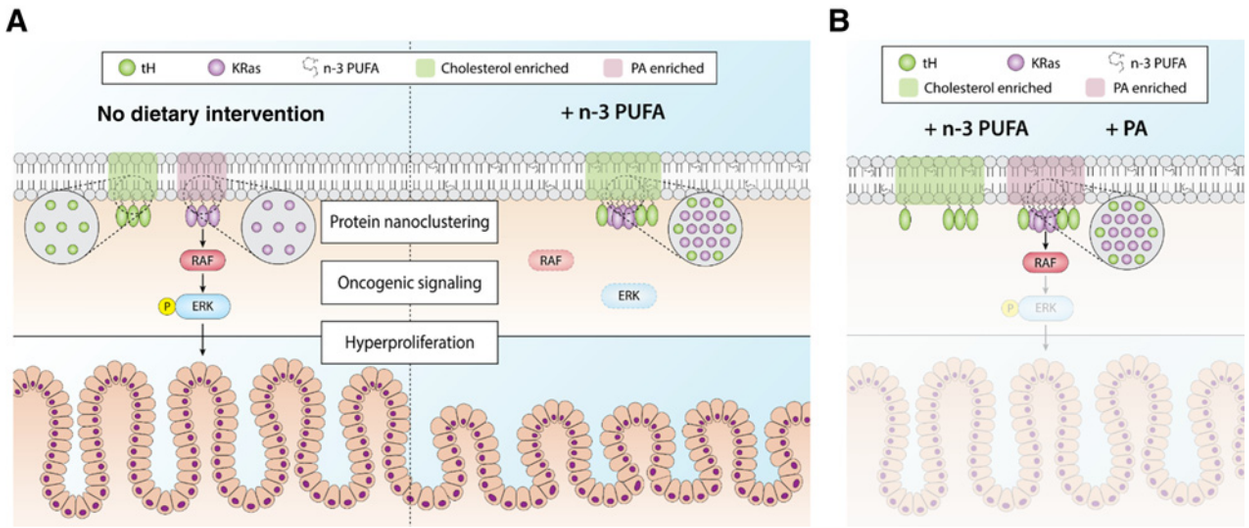

Figure 6.

Summary diagram highlighting n-3 PUFA suppression of oncogenic Ras-mediated signaling and hyperproliferation via disruption of Ras nanoscale proteolipid composition. **A,** Incorporation of long-chain n-3 PUFA into colonocyte plasma membrane phospholipids mislocalizes oncogenic KRas from PA-rich domains into cholesterol-rich but PA-poor domains, generating heterotypic mixed clusters of tH and KRas proteins, thereby disrupting its ability as a nanoswitch to regulate ERK signaling. This results in the suppression of oncogenic Ras-driven phenotypes in the colon. **B,** Exogenous PA restores the lateral segregation of oncogenic KRas from cholesterol-rich domains and the recruitment of Raf.

The plasma membrane contains exquisitely organized and compartmentalized signaling domains, composed of lipids and proteins. A combination of complex biophysical (electrostatic and hydrophobic) interactions between multiple lipid species and membrane proteins, drive the formation of these transient signaling domains (48). With regard to Ras, the highly specific lipid and protein composition of these domains allows selective recruitment of effectors, and therefore is necessary to maintain efficient signal transduction (49). With respect to diet, it has been previously demonstrated that the incorporation of long-chain n-3 PUFA into phospholipids can affect the biophysical properties of the plasma membrane (50). Here, we extend previous studies focusing on membrane biophysical properties, by addressing the impact of n-3 PUFA on the nanoscale localization of lipids and Ras proteins. The lateral segregation and coalescence of Ras proteolipid complexes is likely driven by similar biophysical properties that govern the phase separation of lipids observed in model membranes (51). In addition, the ratios of cholesterol and sphingomyelin influence phase separation (51). This is relevant because dietary n-3 PUFA reduces colonic caveolae cholesterol (25) and T-cell lipid raft sphingomyelin content (26). Furthermore, long-chain n-3 PUFA stabilizes phase separation of membranes generated *in silico* and in cell culture (35, 52). This effect of n-3 PUFA on phase separation is in part dependent on its mol% enrichment in the membrane (52). Therefore, the mol% enrichment of n-3 PUFA in plasma membrane phospholipids is critical to our mechanistic hypothesis. The dose of n-3 PUFA used in our mouse studies is a human equivalent dose of approximately 8.6 g/day, based on body surface area (53). Thus, the mol% enrichment of total n-3 PUFA observed in both our mouse and *Drosophila* models (Fig. 1B; Table 1) is physiologically attainable in humans (47). These studies suggest that the biophysical effects of n-3 PUFA on the plasma membrane may contribute to alterations in Ras lateral segregation in human subjects.

The spatial organization of Ras isoforms into non-overlapping nanometer scale domains on the plasma membrane facilitates the recruitment of Raf, leading to ERK activation (6), thus creating a novel drug target (8). We observed that long-chain n-3 PUFA selectively generate mixed cholesterol-dependent (tH-GFP) and independent (tK-GFP) nanoclusters (Figs. 2G and 4E). This result is similar to the ability of nonsteroidal anti-inflammatory drugs (7) or actin disruption (10) to generate heterotypic mixed clusters. Interestingly, DHA is known to affect actin dynamics (32, 50, 54), which may partially explain the mechanism underlying the formation of heterotypic clusters. Furthermore, the lipid composition of caveolae, which also regulates Ras lateral segregation (55), is modified by long-chain n-3 PUFA (25). Select phospholipid pools such as PS, PA, and phosphatidylinositol-4,5-bisphosphate (PIP_2) are key structural components of Ras nanoclusters (9, 10), and the lateral segregation and heterotypic mixing of H- and KRas is dependent on PS levels in the plasma membrane (10). Interestingly, we have previously demonstrated that dietary fish oil results in the incorporation of EPA and DHA into the acyl chains of PS and to a lesser extent PIP_2 (25, 26, 54). This is noteworthy, because KRas plasma membrane localization and nanoclustering requires specific PS acyl chain species (11), raising the possibility that the altered PS acyl chain profile generated by dietary fish oil may underlie its effects on Ras nanoclustering.

The recruitment of Raf to KRas nanoclusters requires the acidic lipids PA and PS (43, 44). We demonstrate that n-3 PUFA mislocalizes activated KRas to membrane microdomains depleted of PA (Fig. 5H). Notably, the mislocalized KRas predominantly associates with cholesterol-rich domains (Fig. 5K) containing truncated HRas (Fig. 2I). Cholesterol-rich regions of the membrane are suboptimal for Raf activation (36, 46); therefore, these

perturbations result in the failed recruitment of Raf to activated KRas proteolipid assemblies (Fig. 5B and C) and the attenuation of ERK signaling (Figs. 3 and 4H). Importantly, PA-mediated signaling is required for the nuclear activation of ERK (40). Interestingly, exogenous supplementation of PA to DHA-treated cells restores KRasG12V and cholesterol lateral segregation (Fig. 5K), and Raf recruitment (Fig. 5I), without restoring KRasG12V and tH segregation (Fig. 5L). These findings suggest that the heterotypic clustering of KRasG12V and tH does not contribute to the antiproliferative effect of n-3 PUFA. Instead, our data support a mechanistic model in which activated KRas must be associated with a pool of PA in a cholesterol-poor domain of the membrane to recruit Raf and propagate signaling (Fig. 6B). Further research is required to elucidate how exogenous PA can reshape DHA-modified KRas proteolipid complexes.

Although cholesterol is the predominant sterol present in mammalian plasma membranes, ergosterol is the major sterol component present in lower eukaryotes such as *Drosophila* (21). This suggests an evolutionary conserved aspect of membrane organization that even extends to the neural system (18). Therefore, our results using cholesterol-sensitive and -insensitive Ras constructs are interpretable in the *Drosophila* ISC model (Fig. 4C–E). In this *in vivo* study, we also used a functionally active mutated form of Ras1 (RasV12). Interestingly, long-chain n-3 PUFA suppressed Ras1-dependent oncogenic signaling and phenotypes in the fly (Fig. 4F–H), similar to the murine model (Fig. 1). We, therefore, posit that long-chain n-3 PUFA may also alter the nanoscale organization of *Drosophila* Ras1 proteolipid complexes, similar to mammalian KRas (Fig. 6A). However, further work is needed to address this possibility.

In conclusion, our findings mechanistically link the reshaping of Ras proteolipid composition with the ability of n-3 PUFA to attenuate oncogenic Ras-driven colonic hyperproliferation. We propose that our novel observations support the feasibility of using dietary strategies that target plasma membrane organization to reduce Ras oncogenic signaling and cancer risk (28).

Disclosure of Potential Conflicts of Interest

No potential conflicts of interest were disclosed.

Authors' Contributions

Conception and design: N.R. Fuentes, J. Karpac, R.S. Chapkin
Development of methodology: N.R. Fuentes, T.J. Steele, S. Behmer, J. Karpac, R.S. Chapkin
Acquisition of data (provided animals, acquired and managed patients, provided facilities, etc.): N.R. Fuentes, M. Mlih, R. Barhoumi, P. Hardin, T.J. Steele, S. Behmer, J. Karpac
Analysis and interpretation of data (e.g., statistical analysis, biostatistics, computational analysis): N.R. Fuentes, M. Mlih, Y.-Y. Fan, J. Karpac, R.S. Chapkin
Writing, review, and/or revision of the manuscript: N.R. Fuentes, R. Barhoumi, P. Hardin, S. Behmer, I.A. Prior, J. Karpac, R.S. Chapkin
Administrative, technical, or material support (i.e., reporting or organizing data, constructing databases): N.R. Fuentes, R.S. Chapkin
Study supervision: N.R. Fuentes, J. Karpac
Other (provided materials): I.A. Prior

Acknowledgments

We thank J.F. Hancock (UT Health Science Center Houston, TX) for providing transgenic flies carrying UAS expression constructs GPF-tH, RFP-tH, GFP-tK, and RFP-tK; Dr Guangwei Du (UT Health Science Center, Houston, TX) for providing the Spo20-RFP plasmid and Dr. Gregory Fairn (University of Toronto, Canada) for providing the D4H-RFP plasmid. mRFP-Lact-C2 was a gift from Sergio Grinstein (Addgene plasmid # 74061), and mRFP-RBD(R59A)-mRFP was a gift from Karel Svoboda (Addgene plasmid # 18664). We also thank Shigeo Hayashi (Riken Center for Development Biology, Japan) for providing the esg-Gal4 construct and Eric Fearon (Department of Internal Medicine, University of Michigan) for generously donating CDX2P^{creERT}, LSL-K-Ras G12D compound mice, and Rachel Wright for generating the summary diagram. This work was supported by NIH grants R35CA197707 and P30ES023512 and funds from the Allen Endowed Chair in Nutrition & Chronic Disease Prevention. Natividad Fuentes is a recipient of a Predoctoral Fellowship in Pharmacology/Toxicology from the PhRMA Foundation and the National Science Foundation Texas A&M University System Louis Stokes Alliance for Minority Participation (TAMUS LSAMP) Bridge to the Doctorate Fellowship (HRD-1249272).

The costs of publication of this article were defrayed in part by the payment of page charges. This article must therefore be hereby marked *advertisement* in accordance with 18 U.S.C. Section 1734 solely to indicate this fact.

Received February 3, 2018; revised March 26, 2018; accepted May 8, 2018; published first May 16, 2018.

References

1. Cox AD, Fesik SW, Kimmelman AC, Luo J, Der CJ. Drugging the undruggable RAS: Mission Possible? Nat Rev Drug Discov 2014;13:828–51.
2. Stephen AG, Esposito D, Bagni RK, McCormick F. Dragging ras back in the ring. Cancer Cell 2014;25:272–81.
3. Phipps AI, Buchanan DD, Makar KW, Win AK, Baron JA, Lindor NM, et al. KRAS-mutation status in relation to colorectal cancer survival: the joint impact of correlated tumour markers. Br J Cancer 2013;108:1757–64.
4. Herrmann C. Ras-effector interactions: after one decade. Curr Opin Struct Biol 2003;13:122–9.
5. Downward J. Targeting RAS signalling pathways in cancer therapy. Nat Rev Cancer 2003;3:11–22.
6. Tian T, Harding A, Inder K, Plowman S, Parton RG, Hancock JF. Plasma membrane nanoswitches generate high-fidelity Ras signal transduction. Nat Cell Biol 2007;9:905–14.
7. Zhou Y, Cho KJ, Plowman SJ, Hancock JF. Nonsteroidal anti-inflammatory drugs alter the spatiotemporal organization of Ras proteins on the plasma membrane. J Biol Chem 2012;287:16586–95.
8. Cho KJ, Hancock JF. Ras nanoclusters: a new drug target? Small GTPases 2013;4:57–60.
9. Zhou Y, Hancock JF. Ras proteolipid nanoassemblies on the plasma membrane sort lipids with high selectivity. Advances in Biomembranes and Lipid Self-Assembly2017;25:41–62.
10. Zhou Y, Liang H, Rodkey T, Ariotti N, Parton RG, Hancock JF. Signal integration by lipid-mediated spatial cross talk between Ras nanoclusters. Mol Cell Biol 2014;34:862–76.
11. Zhou Y, Prakash P, Liang H, Cho KJ, Gorfe AA, Hancock JF. Lipid-sorting specificity encoded in K-Ras membrane anchor regulates signal output. Cell 2017;168:239–51.e16.
12. Chapkin RS, Akoh CC, Miller CC. Influence of dietary n-3 fatty acids on macrophage glycerophospholipid molecular species and peptidoleukotriene synthesis. J Lipid Res 1991;32:1205–13.
13. Hall MN, Chavarro JE, Lee IM, Willett WC, Ma J. A 22-year prospective study of fish, n-3 fatty acid intake, and colorectal cancer risk in men. Cancer Epidemiol Biomarkers Prev 2008;17:1136–43.
14. Lien EL. Toxicology and safety of DHA. Prostaglandins Leukot Essent Fat Acids 2009;81:125–32.
15. Feng Y, Sentani K, Wiese A, Sands E, Green M, Bommer GT, et al. Sox9 induction, ectopic paneth cells, and mitotic spindle axis defects in mouse colon adenomatous epithelium arising from conditional biallelic Apc inactivation. Am J Pathol 2013;183:493–503.
16. Kim E, Davidson LA, Zoh RS, Hensel ME, Salinas ML, Patil BS, et al. Rapidly cycling Lgr5+ stem cells are exquisitely sensitive to extrinsic dietary factors that modulate colon cancer risk. Cell Death Dis 2016;7:e2460.

17. Habets GG, Knepper M, Sumortin J, Choi YJ, Sasazuki T, Shirasawa S, et al. cDNA array analyses of K-ras-induced gene transcription. Methods Enzymol 2001;332:245–60.
18. Zhou Y, Wong CO, Cho KJ, van der Hoeven D, Liang H, Thakur DP, et al. SIGNAL TRANSDUCTION. Membrane potential modulates plasma membrane phospholipid dynamics and K-Ras signaling. Science 2015; 349:873–6.
19. Piper MD, Blanc E, Leitão-Gonçalves R, Yang M, He X, Linford NJ, et al. A holidic medium for Drosophila melanogaster. Nat Methods 2014; 11:100–5.
20. Shen LR, Lai CQ, Feng X, Parnell LD, Wan JB, Wang JD, et al. Drosophila lacks C20 and C22 PUFAs. J. Lipid Res 2010;51:2985–92.
21. Carvalho M, Sampaio JL, Palm W, Brankatschk M, Eaton S, Shevchenko A. Effects of diet and development on the Drosophila lipidome. Mol Syst Biol 2012;8:600.
22. Jiang H, Grenley MO, Bravo MJ, Blumhagen RZ, Edgar BA. EGFR/Ras/MAPK signaling mediates adult midgut epithelial homeostasis and regeneration in *Drosophila*. Cell Stem Cell 2011;8:84–95.
23. Chang C, Sud D, Mycek M. Fluorescence lifetime imaging microscopy. Methods Cell Biol 2007;81:495–524.
24. Najumudeen AK, Jaiswal A, Lectez B, Oetken-Lindholm C, Guzmán C, Siljamäki E, et al. Cancer stem cell drugs target K-ras signaling in a stemness context. Oncogene 2016;35:5248–62.
25. Ma DW, Seo J, Davidson LA, Callaway ES, Fan YY, Lupton JR, et al. n-3 PUFA alter caveolae lipid composition and resident protein localization in mouse colon. FASEB J 2004;18:1040–2.
26. Fan YY, McMurray DN, Ly LH, Chapkin RS. Dietary (n-3) polyunsaturated fatty acids remodel mouse T-cell lipid rafts. J Nutr 2003;133:1913–20.
27. Turk HF, Barhoumi R, Chapkin RS. Alteration of EGFR spatiotemporal dynamics suppresses signal transduction. PLoS ONE 2012;7:e39682.
28. Fuentes NR, Salinas ML, Kim E, Chapkin RS. Emerging role of chemoprotective agents in the dynamic shaping of plasma membrane organization. Biochim Biophys Acta 2017;1859:1668–78.
29. Kim W, Khan NA, McMurray DN, Prior IA, Wang N, Chapkin RS. Regulatory activity of polyunsaturated fatty acids in T-cell signaling. Prog Lipid Res 2010;49:250–61.
30. Chapkin RS, Wang N, Fan YY, Lupton JR, Prior IA. Docosahexaenoic acid alters the size and distribution of cell surface microdomains. Biochim Biophys Acta 2008;1778:466–71.
31. Prior IA, Muncke C, Parton RG, Hancock JF. Direct visualization of Ras proteins in spatially distinct cell surface microdomains. J Cell Biol 2003; 160:165–70.
32. Turk HF, Monk JM, Fan YY, Callaway ES, Weeks B, Chapkin RS. Inhibitory effects of omega-3 fatty acids on injury-induced epidermal growth factor receptor transactivation contribute to delayed wound healing. Am J Physiol Cell Physiol 2013;304:C905–17.
33. Seo J, Barhoumi R, Johnson AE, Lupton JR, Chapkin RS. Docosahexaenoic acid selectively inhibits plasma membrane targeting of lipidated proteins. FASEB J 2006;20:770–2.
34. Conquer JA, Holub BJ. Effect of supplementation with different doses of DHA on the levels of circulating DHA as non-esterified fatty acid in subjects of Asian Indian background. J Lipid Res 1998;39:286–92.
35. Levental KR, Lorent JH, Lin X, Skinkle AD, Surma MA, Stockenbojer EA, et al. Polyunsaturated lipids regulate membrane domain stability by tuning membrane order. Biophys J 2016;110:1800–10.
36. Prior IA, Harding A, Yan J, Sluimer J, Parton RG, Hancock JF. GTP-dependent segregation of H-ras from lipid rafts is required for biological activity. Nat Cell Biol 2001;3:368–75.
37. Stolze B, Reinhart S, Bulllinger L, Fröhling S, Scholl C. Comparative analysis of KRAS codon 12, 13, 18, 61, and 117 mutations using human MCF10A isogenic cell lines. Sci Rep 2015;5:8535.
38. Prior IA, Lewis PD, Mattos C. A comprehensive survey of Ras mutations in cancer. Cancer Res 2012;72:2457–67.
39. Brunet A, Roux D, Lenormand P, Dowd S, Keyse S, Pouysségur J. Nuclear translocation of p42/p44 mitogen-activated protein kinase is required for growth factor-induced gene expression and cell cycle entry. EMBO J 1999;18:664–74.
40. Zhang F, Wang Z, Lu M, Yonekubo Y, Liang X, Zhang Y, et al. Temporal production of the signaling lipid phosphatidic acid by phospholipase D2 determines the output of extracellular signal-regulated kinase signaling in cancer cells. Mol Cell Biol 2014;34:84–95.
41. Biteau B, Hochmuth CE, Jasper H. Maintaining tissue homeostasis: dynamic control of somatic stem cell activity. Cell Stem Cell 2011;9:402–11.
42. Jiang H, Edgar BA. EGFR signaling regulates the proliferation of Drosophila adult midgut progenitors. Development 2009;136:483–93.
43. Ghosh S, Strum JC, Sciorra VA, Daniel L, Bell RM. Raf-1 kinase possesses distinct binding domains for phosphatidylserine and phosphatidic acid. Phosphatidic acid regulates the translocation of Raf-1 in 12-O-tetradecanoylphorbol-13-acetate-stimulated Madin-Darby canine kidney cells. J Biol Chem 1996;271:8472–80.
44. Ghosh S, Xie WQ, Quest AF, Mabrouk GM, Strum JC, Bell RM. The cysteine-rich region of raf-1 kinase contains zinc, translocates to liposomes, and is adjacent to a segment that binds GTP-ras. J Biol Chem 1994;269:10000–7.
45. Zhou Y, Hancock JF. Ras nanoclusters: versatile lipid-based signaling platforms. Biochim Biophys Acta 2015;1853:841–9.
46. Inder K, Harding A, Plowman SJ, Philips MR, Parton RG, Hancock JF. Activation of the MAPK module from different spatial locations generates distinct system outputs. Mol Biol Cell 2008;19:4776–84.
47. Skarke C, Alamuddin N, Lawson JA, Li X, Ferguson JF, Reilly MP, et al. Bioactive products formed in humans from fish oils. J Lipid Res 2015;56: 1808–20.
48. Sezgin E, Levental I, Mayor S, Eggeling C. The mystery of membrane organization: composition, regulation and roles of lipid rafts. Nat Rev Mol Cell Biol 2017;18:361–74.
49. Zhou Y, Hancock JF. Deciphering lipid codes: K-Ras as a paradigm. Traffic 2018;19:157–65.
50. Kim W, Fan YY, Barhoumi R, Smith R, McMurray DN, Chapkin RS. n-3 polyunsaturated fatty acids suppress the localization and activation of signaling proteins at the immunological synapse in murine CD4+ T cells by affecting lipid raft formation. J Immunol 2008;181:6236–43.
51. Veatch SL, Keller SL. Separation of liquid phases in giant vesicles of ternary mixtures of phospholipids and cholesterol. Biophys J 2003; 85:3074–83.
52. Fan YY, Fuentes NR, Hou TY, Barhoumi R, Li XC, Deutz NEP, et al. Remodelling of primary human CD4+ T cell plasma membrane order by n-3 PUFA. Br J Nutr 2018;119:163–75.
53. Reagan-Shaw S, Nihal M, Ahmad N. Dose translation from animal to human studies revisited. FASEB J 2008;22:659–61.
54. Hou TY, Monk JM, Fan YY, Barhoumi R, Chen YQ, Rivera GM, et al. n-3 polyunsaturated fatty acids suppress phosphatidylinositol 4,5-bisphosphate-dependent actin remodelling during CD4+ T-cell activation. Biochem J 2012;443:27–37.
55. Ariotti N, Fernández-Rojo MA, Zhou Y, Hill MM, Rodkey TL, Inder KL, et al. Caveolae regulate the nanoscale organization of the plasma membrane to remotely control Ras signaling. J Cell Biol 2014;204:777–92.

Published OnlineFirst May 16, 2018; DOI: 10.1158/0008-5472.CAN-18-0324

Cancer Research
The Journal of Cancer Research (1916–1930) | The American Journal of Cancer (1931–1940)

AACR American Association for Cancer Research

Long-Chain n-3 Fatty Acids Attenuate Oncogenic KRas-Driven Proliferation by Altering Plasma Membrane Nanoscale Proteolipid Composition

Natividad R. Fuentes, Mohamed Mlih, Rola Barhoumi, et al.

Cancer Res 2018;78:3899-3912. Published OnlineFirst May 16, 2018.

Supplemental Table 1. *Drosophila* diet fatty acid composition.

Fatty Acid	Holidic Diet	Fish Oil Diet	Corn Oil Diet
	(mol%)	(mol%)	(mol%)
14:0	0.00	12.89	0.00
16:0	0.00	23.27	13.33
16:1n-7	0.00	14.61	0.00
18:0	0.00	3.77	1.87
18:1n-9	0.00	6.82	28.40
18:1n-7	0.00	3.27	0.00
18:2n-6 (LA)	0.00	1.67	55.69
18:3n-3	0.00	1.32	0.71
18:4n-3	0.00	3.40	0.00
20:0	0.00	0.00	0.00
20:3n-6	0.00	0.00	0.00
20:4n-6	0.00	0.00	0.00
20:5n-3 (EPA)	0.00	15.74	0.00
22:0	0.00	0.00	0.00
22:5n-3	0.00	1.60	0.00
22:6n-3 (DHA)	0.00	11.62	0.00

Values represent means from lipids extracted from ~ 1g of experimental diet.

Only selected fatty acids in which at least one observation was > 0.2 mol% are reported.

Supplemental Table 2. Mouse diet composition.

Ingredients	Diet (g/100 g)	
	Corn Oil	Fish Oil
Sucrose	42	42
Casein	20	20
DL-methionine	0.3	0.3
AIN-76 Mineral mix	3.5	3.5
AIN-76 Vitamin mix	1	1
Choline Chloride	0.2	0.2
Corn Starch	22	22
Cellulose	6	6
Fish Oil	0	4
Corn oil	5	1
Total	100	100

Supplemental Table 3. Mouse diet fatty acid composition.

Fatty Acid	Corn Oil (5%)	Fish Oil (4%)
	(mol%)	(mol%)
14:0	0.00	10.23
16:0	13.94	22.46
16:1n-7	0.00	10.13
18:0	1.85	3.80
18:1n-9	27.63	11.12
18:1n-7	0.00	2.61
18:2n-6 (LA)	55.63	10.71
18:3n-3	0.94	1.24
18:4n-3	0.00	2.65
20:0	0.00	0.00
20:3n-6	0.00	0.00
20:4n-6	0.00	0.00
20:5n-3 (EPA)	0.00	12.07
22:0	0.00	0.00
22:5n-3	0.00	1.47
22:6n-3 (DHA)	0.00	11.51

Values represent means from lipids extracted from ~ 1g of experimental diet.

Only selected fatty acids in which at least one observation was > 0.2 mol% are reported.

Supplemental Table 4. Incorporation of exogenous fatty acids into murine colonic crypt membrane phospholipids.

Fatty Acid	Corn Oil Control		Corn Oil + Tamoxifen		Fish Oil + Tamoxifen	
	Mean (mol%)	SEM	Mean (mol%)	SEM	Mean (mol%)	SEM
14:0	8.41	1.65	7.67	1.31	9.43	2.25
16:0	32.39[ab]	0.57	29.99[a]	1.44	33.35[b]	0.97
16:1n-7	2.62	0.24	2.98	0.38	5.05	0.14
18:0	18.25	0.57	17.80	0.79	16.78	0.53
18:1n-9	13.74[a]	0.90	15.78[ab]	1.98	18.34[b]	1.54
18:1n-7	5.18	0.32	4.63	0.55	5.47	0.22
18:2n-6 (LA)	6.96[a]	0.63	7.67[a]	1.07	2.52[b]	0.32
20:0	0.36	0.03	0.48	0.06	0.53	0.07
20:3n-6	2.54	0.13	2.13	0.25	0.37	0.07
20:4n-6	9.15[a]	0.42	5.94[b]	0.68	0.95[c]	0.12
20:5n-3 (EPA)	0.00[a]	0.00	0.00[a]	0.00	3.50[b]	0.88
22:0	0.42	0.02	0.47	0.06	0.68	0.03
22:5n-3	0.00	0.00	0.00	0.00	0.17	0.17
22:6n-3 (DHA)	0.00[a]	0.00	0.00[a]	0.00	2.87[b]	0.51

[a,b,c]Mean values with unlike superscripts within a row were significantly different ($P<0.05$), as determined using one-way ANOVA and uncorrected Fisher's LSD tests.

Values represent mean ± SEM (n = 4 mice per treatment).

Only selected fatty acids in which at least one observation was > 0.2 mol% are reported.

Supplemental Table 5. Incorporation of exogenous corn oil fatty acids into *Drosophila* gut membrane phospholipids.

Fatty Acid	Corn Oil
	(mol%)
14:0	2.11
16:0	21.24
16:1n-7	4.44
18:0	3.92
18:1n-9	23.67
18:1n-7	0.00
18:2n-6 (LA)	40.78
20:0	2.09
20:3n-6	0.00
20:4n-6	1.75
20:5n-3 (EPA)	0.00
22:0	0.00
22:5n-3	0.00
22:6n-3 (DHA)	0.00

Values represent means from pooled Drosophila guts (n=28), grown in two separate vials.

Only selected fatty acids in which at least one observation was > 0.2 mol% are reported.

Supplemental Figure 1. Quantitative image based analysis of pERK. (A) SW48-KRasG12D cells were grown in 8-well glass bottom dishes. Cells were starved (0% FBS) for 18 h in the presence of fatty acid and subsequently stimulated with EGF (25 ng/ml) for 5 min. Cells were then immediately fixed in ice cold 100% methanol. (A) merged DIC and Hoechst images; (B) CellMaskTM Green Plasma Membrane Stain was used to define (C) binary whole cell masks, which was used to create (D) masked images of pERK. Scale bar = 20 µM.

Supplemental Figure 2. Western blot of pERK in the DKOB8 oncogenic KRasG21D overexpression model. Representative western blots from lysates of DKOB8 cells grown in 6-well plates and treated with fatty acid (50 μM) for 72 h. Cells were incubated with ponasterone A (10 μM) for the final 48 h, and then were serum starved (0% FBS) over the final 18 h in the presence of fatty acid or, where indicated, MEK inhibitor (U0126, 10 μM). (A) Incubation with ponasterone A results in a dramatic increase in Ras protein along with pERK. Note that oncogenic KRasG12D is myc-tagged and migrated at a higher molecular weight than the endogenous wild type Ras, which is faintly visible below. (B) Total protein on the membrane was visualized using the Stain Free system (BioRad).

Supplemental Figure 3. Holidic diet containing corn oil does not disrupt Ras spatiotemporal dynamics in *Drosophila* midguts. Nanoclustering-FRET analysis (illustrated in schemes) in *Drosophila* midgut stem cells co-expressing GFP- and RFP-tagged (A) truncated KRas (tK) or (B) truncated HRas (tH). (B and D) 1-2 d old *Drosophila* were placed on holidic diet containing no lipid (red) or corn oil (green) for 5 d prior to dissection. Midguts were mounted for microscopy. In all graphs (B and D), the apparent FRET efficiency was calculated from FLIM data (mean ± SEM, n= (B) 2 or (D) 1 independent experiment(s)). Values in the bars indicate the number of analyzed FOVs. No statistical significance ($P>0.05$) was observed between treatments (n.s.) as determined by an unpaired t-test.

Supplemental Figure 1

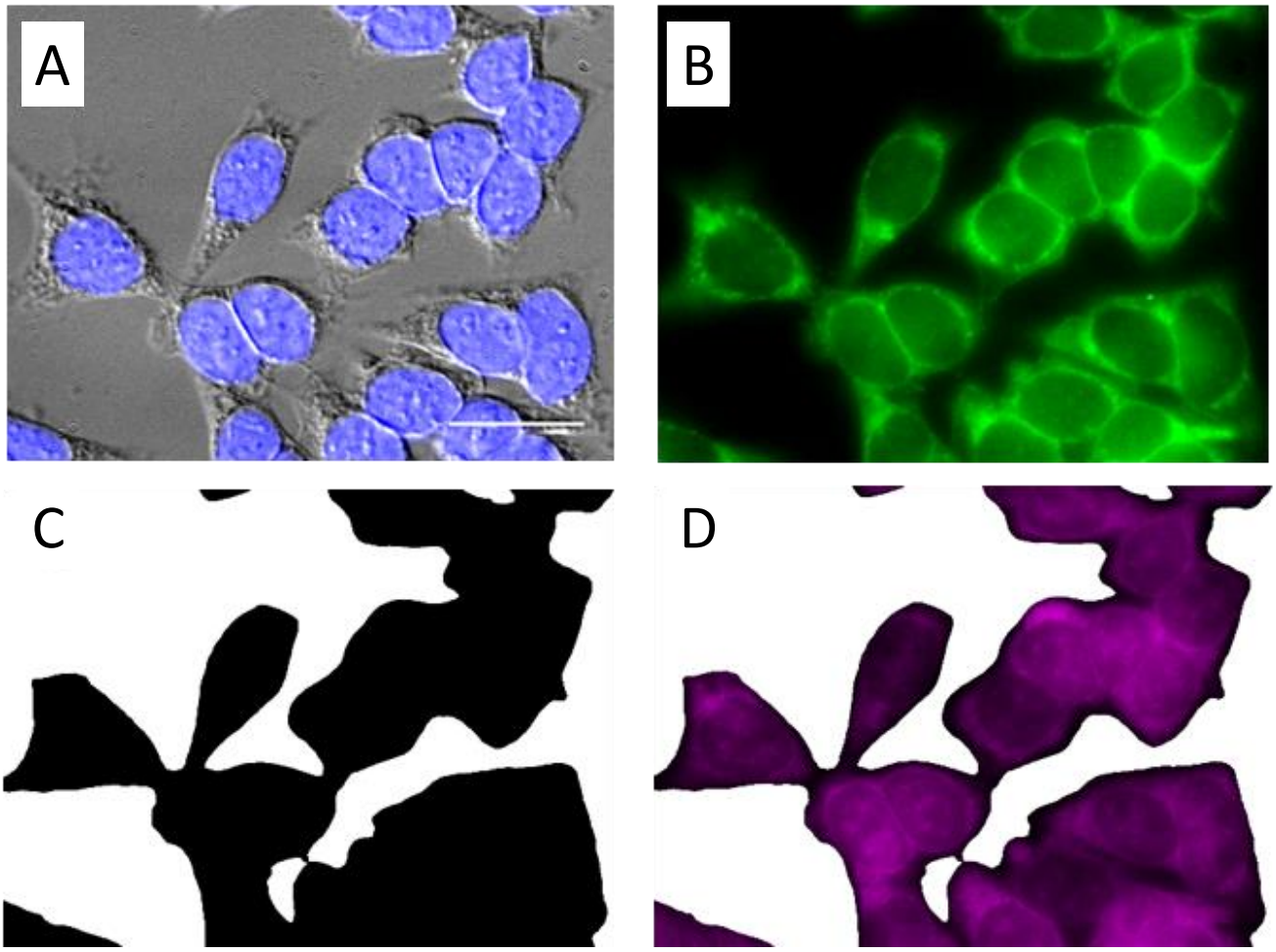

Supplemental Figure 2

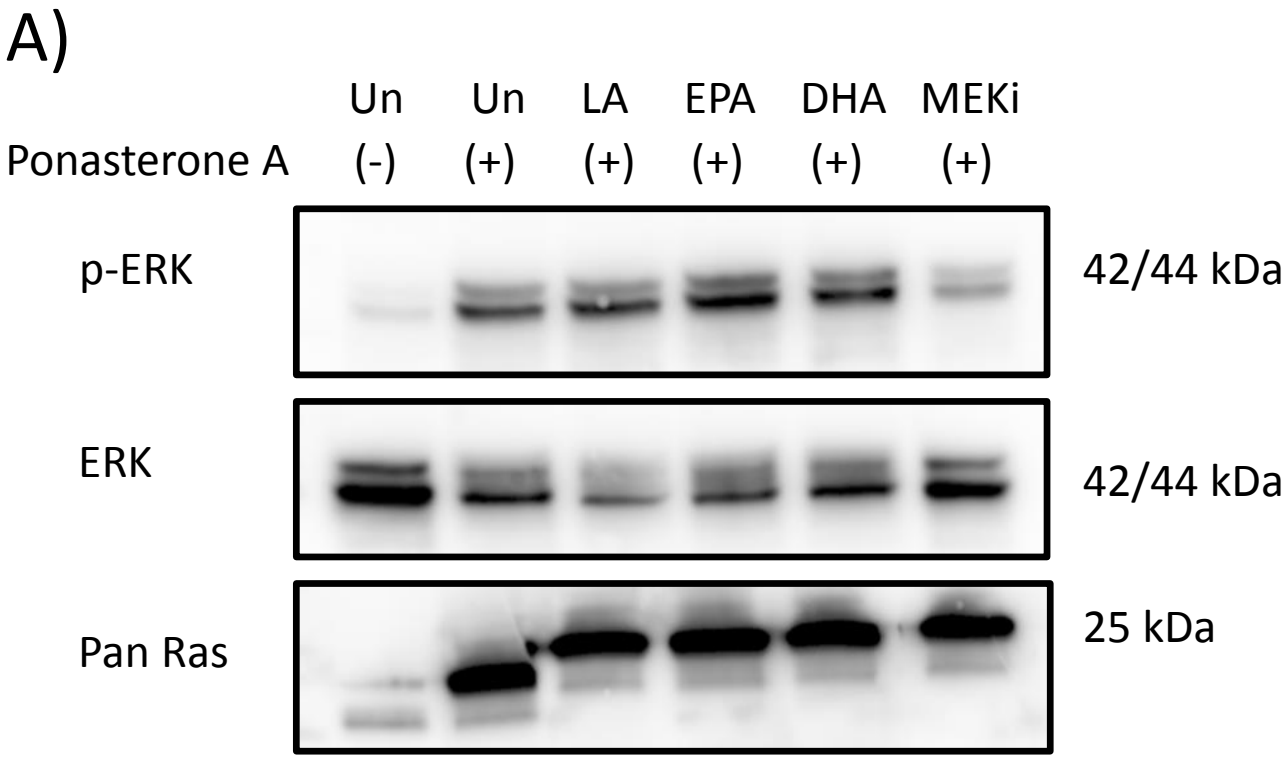

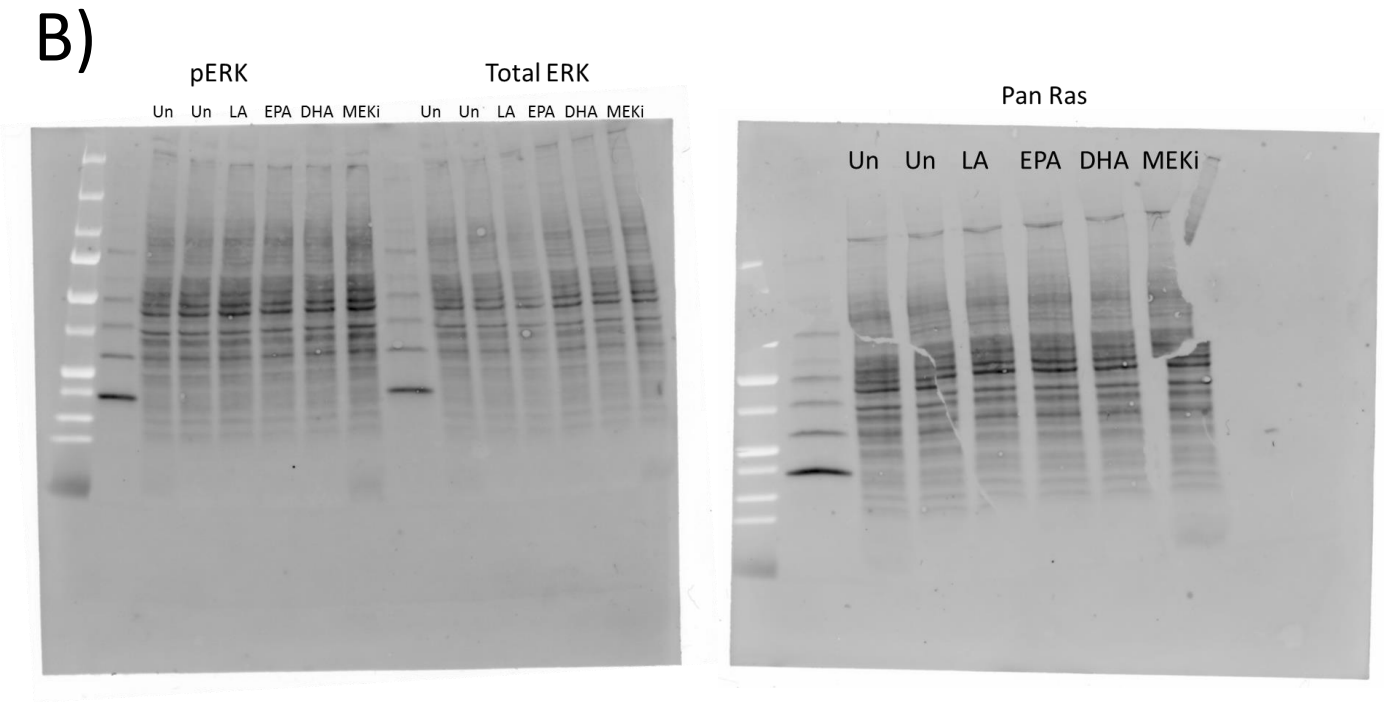

Supplemental Figure 3